AWARD NUMBER: **W81XWH-15-1-0493**

TITLE: **Targeting Neuromimicry in Prostate Cancer Metastasis**

PRINCIPAL INVESTIGATOR: **Boyang Wu, Ph.D.**

CONTRACTING ORGANIZATION: **Cedars-Sinai Medical Center**
Los Angeles, CA 90048

REPORT DATE: **October 2016**

TYPE OF REPORT: **Annual**

PREPARED FOR: **U.S. Army Medical Research and Materiel Command**
Fort Detrick, Maryland 21702-5012

DISTRIBUTION STATEMENT: **Approved for Public Release;**
Distribution Unlimited

The views, opinions and/or findings contained in this report are those of the author(s) and should not be construed as an official Department of the Army position, policy or decision unless so designated by other documentation.

REPORT DOCUMENTATION PAGE

Form Approved
OMB No. 0704-0188

1. REPORT DATE	2. REPORT TYPE	3. DATES COVERED
October 2016	Annual Report	15 Sep 2015 - 14 Sep 2016

4. TITLE AND SUBTITLE

Targeting Neuromimicry in Prostate Cancer Metastasis

5a. CONTRACT NUMBER

5b. GRANT NUMBER
W81XWH-15-1-0493

5c. PROGRAM ELEMENT NUMBER

6. AUTHOR(S)
Boyang Wu

E-Mail: boyang.wu@wsu.edu

5d. PROJECT NUMBER

5e. TASK NUMBER

5f. WORK UNIT NUMBER

7. PERFORMING ORGANIZATION NAME(S) AND ADDRESS(ES)

Cedars-Sinai Medical Center
8700 Beverly Blvd
Los Angeles, CA 90048-1804

8. PERFORMING ORGANIZATION REPORT NUMBER

9. SPONSORING / MONITORING AGENCY NAME(S) AND ADDRESS(ES)

U.S. Army Medical Research and Materiel Command
Fort Detrick, Maryland 21702-5012

10. SPONSOR/MONITOR'S ACRONYM(S)

11. SPONSOR/MONITOR'S REPORT NUMBER(S)

12. DISTRIBUTION / AVAILABILITY STATEMENT

Approved for Public Release; Distribution Unlimited

13. SUPPLEMENTARY NOTES

14. ABSTRACT

The purpose of this project is to investigate the functional and mechanistic roles of a neural enzyme monoamine oxidase A (MAOA) and its downstream neuronal factors in mediating prostate cancer-nerve reciprocal interactions and prostate cancer metastasis. Throughout the Year 1 of this study, we established and validated a series of stable wild-type control, MAOA-overexpressing, and MAOA-knockdown human prostate cancer cells which were further subjected to stable labeling of fluorescence protein and luciferase for subsequent visualization of MAOA-mediated prostate cancer-never cell communication in vitro and in vivo. We also demonstrated that MAOA significantly promoted prostate tumor growth and metastasis to distant organs, including intestine, liver and lung, in different orthotopic xenograft mouse models. In addition, we showed that MAOA inhibitor clorgyline effectively inhibited prostate tumor growth and progression in mice.

15. SUBJECT TERMS

Prostate cancer, monoamine oxidase A, neuropilin1, metastasis, clorgyline, xenograft mouse models

16. SECURITY CLASSIFICATION OF:			17. LIMITATION OF ABSTRACT	18. NUMBER OF PAGES	19a. NAME OF RESPONSIBLE PERSON
a. REPORT	b. ABSTRACT	c. THIS PAGE			USAMRMC
Unclassified	Unclassified	Unclassified	Unclassified	47	19b. TELEPHONE NUMBER *(include area code)*

Standard Form 298 (Rev. 8-98)
Prescribed by ANSI Std. Z39.18

Table of Contents

1. INTRODUCTION: Monoamine oxidase A (MAOA), **the subject of the present study**, is a key neural enzyme that metabolizes monoamine neurotransmitters and regulates neurotransmission, neural circuits and brain function. We found that MAOA is increased in high-grade and metastatic prostate cancer (PCa), particularly associated with perineural invasion (PNI), which may be mediated via MAOA's downstream neurotrophic and axon guidance factors, including neuropilin 1 (NRP1). **The purpose of this research** is twofold: 1) to define the functional and mechanistic roles of the MAOA/NRP1 axis in mediating PCa-nerve reciprocal interactions and PCa metastasis, and 2) to evaluate the effectiveness of targeting the MAOA/NRP1 axis by pharmacological approaches on disrupting tumor-nerve interactions and abrogating PCa invasion and metastasis in PCa cell co-culture and xenograft mouse models. **The scope of this research** involves experiments and assays to study the roles of MAOA and its associated neuronal genes in PCa progression and metastasis in vitro (PC-3, C4-2, $ARCaP_M$ and CWR22Rv1 cells, which are all androgen-insensitive and metastatic) and in vivo (PNI and nerve-facilitated metastasis to distant organs).

2. KEYWORDS: prostate cancer (PCa), monoamine oxidase A (MAOA), neuropilin1 (NRP1), metastasis, clorgyline, xenograft mouse models.

3. ACCOMPLISHMENTS:

- **What were the major goals of the project?**
  The progress during the Year 1 of this project in accordance with the detailed task assignments as presented in SOW, with slight adjustments, is described below:

  Major Task 1 (**Specific Aim 1**): To determine whether and how the MAOA/NRP1 axis mediates PCa-nerve interactions in cell co-culture models.

Subtask 1: Establish and validate PCa stable cell lines (PC-3, C4-2, $ARCaP_M$ and CWR22Rv1) subjected to viral infection with Luc/GFP-expressing lentiviral particles, followed by genetic manipulation of MAOA and NRP1 expression by either plasmid-based overexpression or shRNA-mediated silencing.	Months 1-4	Dr. Wu [CSMC]

  Major Task 2 (**Specific Aim 1**): To determine the effect of the MAOA/NRP1 axis on tumor-nerve interactions and PCa metastasis in orthotopic xenograft mouse models.

Subtask 1: Establish prostate tumors (PC-3 and $ARCaP_M$) in male SCID mice by orthotopic injection, monitor tumor growth, local invasion and distant metastasis in mice by in vivo bioluminescence imaging for 10-12 weeks, and confirm tumor metastases by necropsy and ex vivo bioluminescence imaging at the experiment endpoint.	Months 5-8	Dr. Wu [CSMC]

  Major Task 4 (**Specific Aim 2**): To evaluate the effectiveness of MAOA inhibitor clorgyline on abrogating prostate tumor invasion and metastasis in orthotopic tumor xenograft mouse models.

Subtask 1: Establish prostate tumors ($ARCaP_M$ and CWR22Rv1) in male SCID mice by orthotopic injection, followed by 10-week treatment of MAOA inhibitor clorgyline, monitor tumor growth, local invasion and distant metastasis in	Months 9-12	Dr. Wu [CSMC]

mice by in vivo bioluminescence imaging in the treatment period, and confirm tumor metastases by necropsy and ex vivo bioluminescence imaging at the experiment endpoint.

Major Task 2, Subtask 1 and Major Task 4, Subtask 1 were performed ahead of schedule as outlined in the original SOW to parallel animal studies described in the manuscript attached to the Appendices (see detailed explanations in CHANGES/PROBLEMS section below). The related changes were made in the revised SOW accordingly.

- **What was accomplished under these goals?**

1) Major activities:

Major Task 1, **Subtask 1**: We established and validated a series of human PCa cell lines, which were subjected to stable dual labeling of fluorescence protein and luciferase (Luc) and further to manipulation of MAOA/NRP1 expression levels, for subsequent cell co-culture and animal studies. These cell lines include: a) control and MAOA-overexpressing (OE) GFP/Luc-labeled PC-3 cells, b) control and MAOA-OE GFP/Luc-labeled CWR22Rv1 cells, c) control and MAOA-knockdown (KD) RFP/Luc-labeled C4-2 cells, d) control and MAOA-KD RFP/Luc-labeled $ARCaP_M$ cells, e) control and NRP1-OE GFP/Luc-labeled PC-3 cells, and f) control, NRP1-KD, MAOA-OE and MAOA-OE/NRP1-KD PC-3 cells. We stably transfected the MAOA or NRP1 expression construct into PC-3 or CWR22Rv1 cells followed by neomycin selection, which were further subjected to infection with lentiviral particles co-expressing GFP and luciferase (GenTarget) followed by puromycin selection. An empty vector was stably transfected in control cells. We stably transfected the pASRed2 expression vector (Clontech), encoding a variant AsRed2 Anemonia sulcata RFP, into C4-2 and $ARCaP_M$ cells followed by neomycin selection, which were further subjected to infection with lentiviral particles expressing MAOA-targeting shRNAs (Sigma-Aldrich) followed by puromycin selection. Lentiviral particles expressing a non-targeting shRNA were used for infection in control cells. C4-2 and $ARCaP_M$ cells were also infected with house-made retrovirus expressing the MSCV luciferase PGK vector (Promega) followed by hygromycin selection for stable labeling of a luciferase gene. NRP1 KD was achieved in PC-3 cells in the absence or presence of MAOA OE by infection with lentiviral particles expressing NRP1-targeting shRNAs (Santa Cruz). All stable cells were maintained in culture media supplemented with different selective antibiotics at the same doses used for selection prior to the formal experiments. Different manipulations of MAOA and/or NRP1 expression levels were examined by Western blot (Figure 1, see below). Stable labeling of fluorescence proteins and luciferase were validated by fluorescence microscopy and luciferase assays, respectively (Figure 2, see below). These cells are now ready to be used in the proposed cell line and animal studies.

Major Task 2, **Subtask 1**: We established orthotopic xenograft mouse models by directly injecting luciferase-tagged PCa cells, a) control and MAOA-OE PC-3, and b) control and MAOA-KD $ARCaP_M$, into the prostate of SCID mice, and monitored tumor growth and metastasis by bioluminescence imaging (BLI) weekly for up to 11 weeks. Metastases were also confirmed by necropsy and ex vivo BLI at the experiment endpoint (Figure 3, see below).

Major Task 4, **Subtask 1**: We established orthotopic xenograft mouse models by directly injecting luciferase-tagged PCa cells, a) control and MAOA-KD $ARCaP_M$, and b) control and MAOA-KD CWR22Rv1, into the prostate of SCID mice, followed by BLI measurement

of tumor growth. Mice were randomly assigned to 2 groups for treatment based on BLI signals of prostate tumors 2 weeks after tumor inoculation. Intraperitoneal (i.p.) injection of clorgyline (30 mg/kg) was given to mice every other day for 6 weeks, with saline injection for the control group. Development of metastasis was monitored by BLI weekly. Metastases were also confirmed by necropsy at the experiment endpoint (Figure 4, see below).

2) Specific objectives:

Major Task 1, **Subtask 1**: To establish and validate MAOA/NRP1-manipulated PCa cells with stable labeling of fluorescence protein and Luc for subsequently visualizing MAOA/NRP1-mediated PCa-nerve cell interactions in vitro and in vivo.

Major Task 2, **Subtask 1**: To determine the effect of MAOA and its downstream effectors, particularly NRP1, on PCa growth and metastasis in orthotopic xenograft mouse models.

Major Task 4, **Subtask 1**: To evaluate the effectiveness of MAOA inhibitor clorgyline on abrogating prostate tumor growth and metastasis in orthotopic xenograft mouse models.

3) Significant results or key outcomes:

Major Task 1, **Subtask 1**: We successfully established all the proposed PCa cells bearing different manipulations of MAOA/NRP1 expression levels, which were validated by Western blot (Figure 1). In addition, these cells were stably labeled with GFP/RFP and Luc, which were detected by fluorescence microscopy and luciferase assays, respectively. As determined by luciferase assays, enforced expression of MAOA increased PC-3 cell proliferation by 97% while genetic silencing of MAOA reduced C4-2 cell proliferation by 27%, both over a 6-day period, which is consistent with our previous observations measured by cell counting assays (Figure 2).

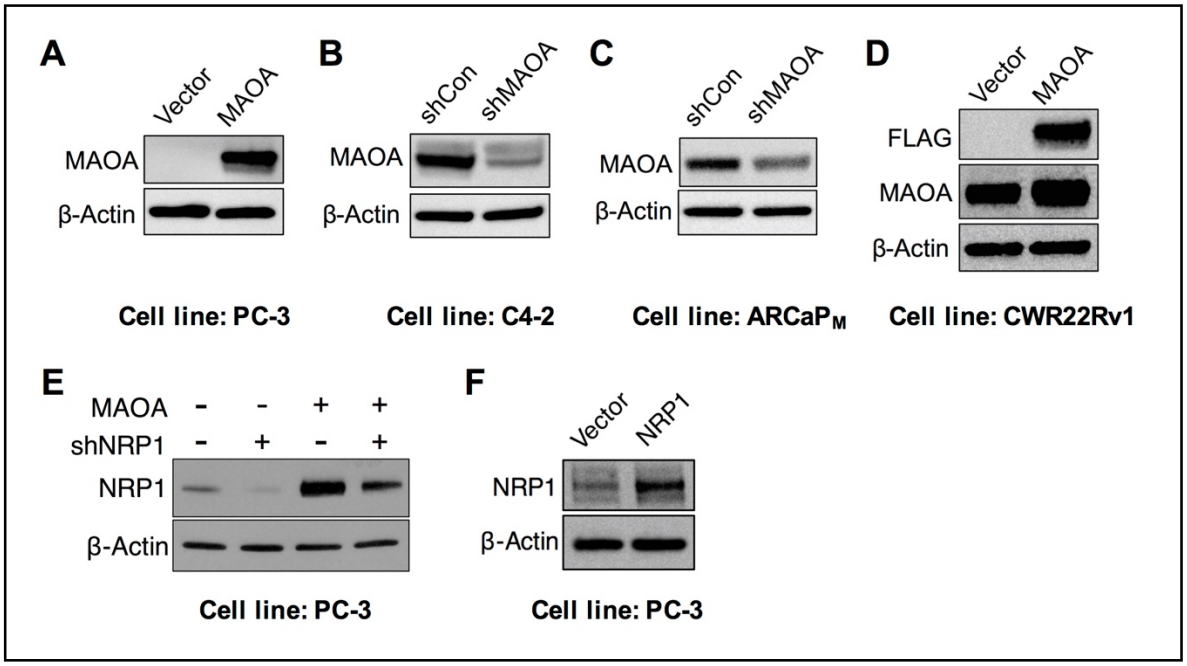

Figure 1. (A-F) Western blotting analysis of MAOA and NRP1 protein levels in indicated PCa cells. Vector, control for MAOA OE or NRP1 OE; MAOA, MAOA OE; shCon, control for MAOA KD; shMAOA, MAOA KD; shNRP1, NRP1 KD; NRP1, NRP1 OE.

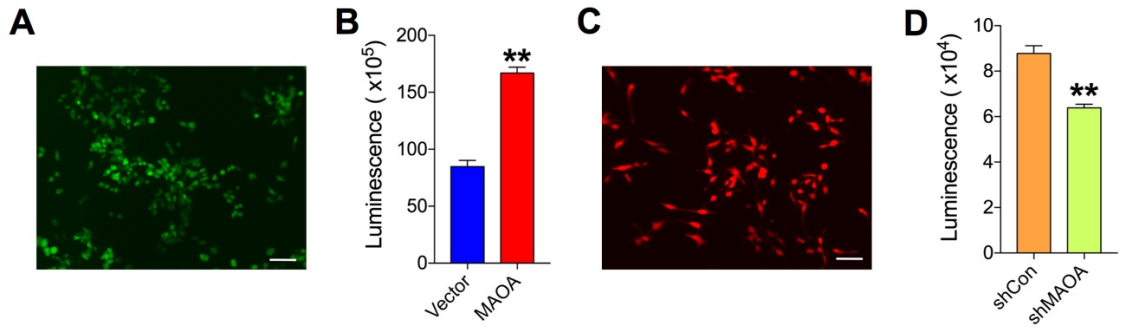

Figure 2. Characterization of Luc- and GFP/RFP-expressing PCa cells. (A) A representative image of GFP-tagged PC-3 cells captured by fluorescence microscopy. Scale bar: 100 μm. (B) Cell proliferation of Luc-tagged control and MAOA-OE PC-3 cells cultured for 6 days as measured by luciferase assays. (C) A representative image of RFP-tagged C4-2 cells captured by fluorescence microscopy. Scale bar: 100 μm. (D) Cell proliferation of Luc-tagged control and MAOA-KD C4-2 cells cultured for 6 days as measured by luciferase assays. Data represent the mean ± SEM. ** p<0.01.

Major Task 2, **Subtask 1**: We showed that MAOA OE in PCa cells significantly promoted prostate tumor growth, particular metastasis to distant organs, such as lung, compared to control cells. Genetic KD of MAOA in PCa cells markedly lowered tumor growth and distant metastasis, such as intestine and liver (Figure 3).

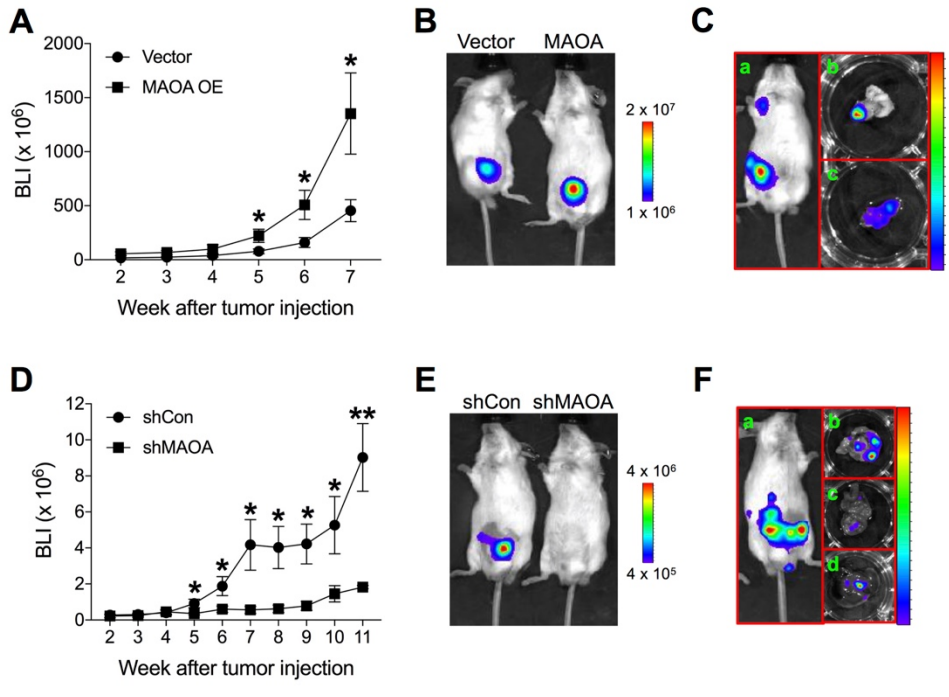

Figure 3. MAOA promotes PCa tumor growth and metastasis in orthotopic xenograft mouse models. (A) Growth curves of control and MAOA-OE PC-3 prostate tumors as measured by BLI in mice (n=7 per group). (B) BLI images of a representative mouse from each group in (A). (C) BLI images of a representative mouse developing distant metastasis in MAOA-OE group. Both the whole-body in vivo (a) and select organ-specific metastasis ex vivo (b, prostate tumor; c, lung metastases) images are shown. BLI scales (unit, radiance): a, 1 x 10^5 - 1 x 10^6; b-c, 1 x 10^6 - 2 x 10^7. (D) Growth curves of control and MAOA-KD ARCaP$_M$ prostate tumors as measured by BLI in mice (n=6 per group). (E) BLI images of a representative mouse from each group in (D). (F) BLI images of a representative mouse developing distant metastasis in control group. Both the whole-body in vivo (a) and select organ-specific distant metastases ex vivo (b, prostate tumor; c, intestine; d, liver) images are shown. BLI scales (unit, radiance): a, 1 x 10^5 - 6 x 10^5; b-c, 2 x 10^5 - 4 x 10^6; d, 2 x 10^4 - 4 x 10^5. Data represent the mean ± SEM. * p<0.05, ** p<0.01.

Major Task 4, **Subtask 1**: We demonstrated the efficacy of clorgyline, a small molecule irreversible MAOA inhibitor, in inhibiting prostate tumor growth and progression in 2 PCa xenograft models, ARCaP$_M$ and CWR22Rv1 (Figure 4).

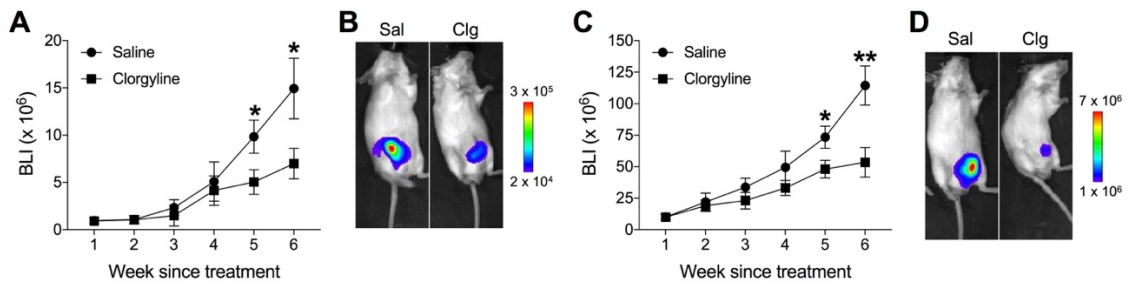

Figure 4. Clorgyline treatment reduced prostate tumor growth and progression in orthotopic xenograft mouse models. (A) Growth curves of saline- and clorgyline-treated ARCaP$_M$ prostate tumors as measured by BLI in mice (n=7 per group). (B) BLI images of a representative mouse from each group in (A). (C) Growth curves of saline- and clorgyline-treated CWR22Rv1 prostate tumors as measured by BLI in mice (n=8 per group). (D) BLI images of a representative mouse from each group in (C). Data represent the mean ± SEM. * p<0.05, ** p<0.01.

4) Other achievements: Nothing to Report.

- **What opportunities for training and professional development has the project provided?**
  Nothing to Report.

- **How were the results disseminated to communicates of interest?**
  Nothing to Report.

- **What do you plan to do during the next reporting period to accomplish the goals?**

  As outlined in the revised SOW, I will continue to work on this project in my new institution, WSU, with special emphasis on two areas: 1) to analyze tumor samples collected from all aforementioned animal studies, including tumor histopathology, tumor cell

proliferation/apoptosis, tumor expression of MAOA/NRP1 and other related neuronal factors, and nerve density, by IHC staining and TUNEL assay (Months 13-20); 2) to set up 2D/3D PCa cell-DRG neuron co-culture models and study MAOA's role in mediating PCa-nerve reciprocal interactions by different cell-based assays using the PCa cells already established (Months 21-24). These studies will provide direct insights into the functional and mechanistic role of MAOA and its downstream neuronal factors in mediating PCa-nerve communication along PCa progression and metastasis.

4. IMPACT:

- **What was the impact on the development of the principal discipline(s) of the project?**

  Our findings have so far clearly demonstrated MAOA's role in promoting PCa progression and metastasis in orthotopic xenograft models, which was supported by the effectiveness of MAOA inhibitors in reducing prostate tumor growth and progression in mice. These results provide evidence on MAOA's function in mediating extraprostatic extension of PCa cells, accompanied by nerve- and other alternative route(s)-facilitated PCa cell spread, and lay foundations for further exploring the underlying molecular mechanisms.

- **What was the impact on other disciplines?**
  Nothing to Report.

- **What was the impact on technology transfer?**
  Nothing to Report.

- **What was the impact on society beyond science and technology?**
  Nothing to Report.

5. CHANGES/PROBLEMS:

- **Changes in approach and reasons for change:** We performed animal studies in orthotopic xenograft models, Major Task 2, Subtask 1 and Major Task 4, Subtask 1, ahead of schedule as outlined in the original SOW (Months 15-18 and 26-29), which was aimed to parallel another set of animal experiments in intracardiac xenograft models in an alternative study for making comparisons. By this approach, we were able to understand MAOA's role in mediating PCa metastasis in a more comprehensive way by using different xenograft models (othotopic vs. intracardiac). We have included the other study in the Appendices below. We have revised the SOW accordingly, and will continue to work on all proposed tasks in the next 2 years.

- **Actual or anticipated problems or delays and actions or plans to resolve them:** Nothing to Report.

- **Changes that had a significant impact on expenditures:** Nothing to Report.

- **Significant changes in use or care of human subjects, vertebrate animals, biohazards, and/or select agents**: Nothing to Report.

6. PRODUCTS:

- **Publications, conference papers, and presentations**

- **Journal publications:**
  Wu JB*, Yin L, Shi C, Li Q, Duan P, Huang JM, Liu C, Wang F, Lewis M, Wang Y, Lin TP, Pan CC, Posadas EM, Zhau HE, Chung LW*. (2016) MAOA-dependent activation of sonic hedgehog-IL6-RANKL signaling network promotes prostate cancer metastasis by engaging tumor-stromal cell interactions. (*co-corresponding author) *Cancer Cell*, Accepted.

- **Books or other non-periodical, one-time publications:** None.

- **Other publications, conference papers, and presentations:**
  Conference abstracts:
  Wu JB, Zhau HE, Chung LW. (11/2015) Monoamine oxidase A promotes prostate cancer neuromimicry by activation of axon guidance genes. *The Society for Basic Urologic Research (SBUR) 2015 Fall Symposium*. Fort Lauderdale, FL.

  Wu JB, Li Q, Chu GC, Zhau HE. (8/2016) Monoamine oxidase A promotes prostate cancer neuromimicry by activation of neurotrophic and axon guidance genes. *US Army Medical Research and Material Command Congressionally Directed Medical Research Programs (CDMRP) Prostate Cancer Research Program (PCRP) Innovative Minds in Prostate Cancer Today (IMPaCT) Young Investigators Meeting*. Towson, MD.

  Presentations:
  Wu JB. "Exploring and Targeting Neuromimicry in Prostate Cancer". North Dakota State University School of Pharmacy, Fargo, ND. (01/2016)

  Wu JB. "Exploring and Targeting Neuromimicry in Prostate Cancer". Washington State University College of Pharmacy, Spokane, WA. (01/2016)

  Wu JB. "Exploring and Targeting Neuromimicry in Prostate Cancer". Department of Pharmacology and Toxicology, Indiana University School of Medicine, Indianapolis, IN. (02/2016)

- **Website(s) or other Internet site(s):** None.

- **Technologies or techniques:** None.

- **Inventions, patent applications, and/or licenses:** None.

- **Other Products:** None.

7. PARTICIPANTS & OTHER COLLABORATING ORGANIZATIONS

- **What individuals have worked on the project?**

Name:	Boyang (Jason) Wu, Ph.D.
Project Role:	PI
Research Identifier (e.g. ORCID ID):	Not applicable
Nearest person month worked:	8

Contribution to Project:	Dr. Wu performed work on establishment of all PCa cell lines and animal studies described above.
Funding Support	NIH/NCI 2P01CA098912

Name:	Chunyan Liu
Project Role:	Research Technician
Research Identifier (e.g. ORCID ID):	Not applicable
Nearest person month worked:	3
Contribution to Project:	Ms. Liu performed work on validation of established PCa cell lines.
Funding Support:	NIH/NCI 2P01CA098912

- **Has there been a change in the active other support of the PD/PI(s) or senior/key personnel since the last reporting period?**
  Nothing to Report.

- **What other organizations were involved as partners?**
  Nothing to Report.

8. SPECIAL REPORTING REQUIREMENTS

- **COLLABORATIVE AWARDS:** Not Applicable.

- **QUAD CHARTS:** Not Applicable.

9. APPENDICES: Original copies of meeting abstracts and journal articles, including 1) 2015 SBUR conference abstract, 2) 2016 DoD CDMRP PCRP IMPaCT conference abstract, and 3) Cancer Cell manuscript in acceptance version.

Monoamine oxidase A promotes prostate cancer neuromimicry by activation of axon guidance genes

Jason Boyang Wu, Haiyen E. Zhau, and Leland W.K. Chung

Uro-Oncology Research Program, Department of Medicine, Cedars-Sinai Medical Center, Los Angeles, CA 90048

Background: Perineural invasion (PNI), a complex process of neoplastic nerve invasion, has been recognized as a significant route for prostate cancer (PCa) metastasis and associated with poor clinical outcomes. Recent studies, including ours, have shown that PCa cells develop neuromimicry by expressing neuronal genes and exhibiting neuron-like phenotypes, which enable cancer cells to mimic and reciprocally interact with nerves to promote metastatic spread in and along nerves. This represents a new opportunity to develop novel therapeutics for PCa metastasis.

Methods: PCa tissue microarrays (N=74) were used for immunohistochemical and quantum dot labeling analyses of monoamine oxidase A (MAOA) expression, a key enzyme metabolizing monoamine neurotransmitters, to explore its association with PNI. A separate clinical cohort of both early and late-stage PCa cases (N=65), including paired normal/tumor tissues, underwent whole-genome and -transcriptome sequencing analysis to identify novel disease-related genetic alterations. MAOA overexpression in human PCa PC-3 cells allowed us to determine the expression of downstream genes mediating axonal growth and migration by qPCR, Western blot and ELISA. The expression of select adrenergic and cholinergic receptors known to promote PNI and PCa metastasis was also assessed in prostate stromal cells from wild-type/MAOA-knockout and vehicle-/clorgyline (a MAOA inhibitor) treated mice by qPCR.

Results: Increased tumor MAOA expression was associated with PNI in PCa patient samples, with intense expression observed in 1) nerve-invasive tumor areas in the entire cohort and 2) PNI areas relative to other non-PNI cancerous areas in the same patient sample. Sequencing analysis identified axon guidance pathway genes, such as semaphorin signaling-related genes, to have the highest genetic alteration rate in >70% samples. Overexpression of MAOA increased the secretion of nerve growth factor by 3-4 fold and also activated select class 3 semaphorin signaling molecules, including semaphorin 3C, Plexin A2 and neuropilin 1 (NRP1), which act as the ligand, receptor and co-receptor respectively, in PC-3 cells. We further confirmed a positive co-expression correlation between MAOA and NRP1 in clinical samples and demonstrated that NRP1 is a downstream effector mediating MAO's function in PCa cells. Additionally, genetic deletion or pharmacological inhibition of MAOA in mouse prostate stromal cells reduced the expression of select adrenergic (Adrβ2 and Adrβ3) and cholinergic (Chrm1) receptors.

Conclusions: We demonstrated that MAOA and its associated axon guidance genes induce PCa neuromimicry, and may serve as a driver promoting perineural PCa metastasis.

This work was supported by NIH/NCI grants 2P01CA098912 and R01CA122602, the Board of Governors Cancer Research Chair, the Steven Spielberg Fund in Prostate Cancer Research, and a Margaret E. Early Medical Research Trust Award (to L.W.K.C.); Department of Defense Prostate Cancer Research Program grant PC140278 (to J.B.W. and H.E.Z.). We thank Mr. Gary Mawyer for editorial assistance.

Monoamine Oxidase A Promotes Prostate Cancer Neuromimicry by Activation of Neurotrophic and Axon Guidance Genes

Boyang (Jason) Wu, Qinlong Li, Gina Chia-Yi Chu, and Haiyen E. Zhau

BW: BoyangJaosn.Wu@cshs.org, Cedars-Sinai Medical Center
QL: qinlongli@163.com, Cedars-Sinai Medical Center
GCC: Chia-Yi.Chu@cshs.org, Cedars-Sinai Medical Center
HEZ: Haiyen.Zhau@cshs.org, Cedars-Sinai Medical Center

Background and Ojectives: Perineural invasion (PNI), a complex process of neoplastic nerve invasion, has been recognized as a significant route for prostate cancer (PCa) metastasis and associated with poor clinical outcomes. Recent studies, including ours, have shown that PCa cells develop neuromimicry by expressing neuronal genes and exhibiting neuron-like phenotypes, which enable cancer cells to mimic and reciprocally interact with nerves to promote metastatic spread in and along nerves. This represents a new opportunity to develop novel therapeutics for PCa metastasis.

Methodologies: PCa tissue microarrays (N=74) were used for immunohistochemical and quantum dot labeling (QDL) analyses of monoamine oxidase A (MAOA) expression, a key enzyme metabolizing monoamine neurotransmitters, to explore its association with PNI. A separate clinical cohort of both early and late-stage PCa cases (N=65), including paired normal/tumor tissues, underwent whole-genome and -transcriptome sequencing analysis to identify novel disease-related genetic alterations. MAOA overexpression in human PCa PC-3 cells allowed us to determine the expression of downstream genes mediating axonal growth and migration by qPCR, Western blot and ELISA. The expression of select adrenergic and cholinergic receptors known to promote PNI and PCa metastasis was also assessed in prostate stromal cells from wild-type/MAOA-knockout and vehicle-/clorgyline (a MAOA inhibitor) treated mice by qPCR. In addition, orthotopic xenograft models were established by using PC-3 (vector and MAOA-overexpression) and $ARCaP_M$ (control and MAOA-knockdown) PCa cells to determine MAOA-mediated prostate tumor growth, invasion and metastases in mice, with nerve fiber densities within tumors further assessed by QDL analyses of nerve-specific markers.

Results: Increased tumor MAOA expression was associated with PNI in PCa patient samples, with intense expression observed in 1) nerve-invasive tumor areas in the entire cohort and 2) PNI areas relative to other non-PNI cancerous areas in the same patient sample. Sequencing analysis identified axon guidance pathway genes, such as semaphorin signaling-related genes, to have the highest genetic alteration rate in >70% samples. Overexpression of MAOA increased the secretion of nerve growth factor by 3-4 fold and also activated select class 3 semaphorin signaling molecules, including semaphorin 3C, Plexin A2 and neuropilin 1 (NRP1), which act as the ligand, receptor and co-receptor respectively, in PC-3 cells. We further confirmed a positive co-expression correlation between MAOA and NRP1 in clinical samples and demonstrated that NRP1 is a downstream effector mediating MAO's function in PCa cells. Additionally, genetic deletion or pharmacological inhibition of MAOA in mouse prostate stromal cells reduced the expression of select adrenergic (Adrβ2 and Adrβ3) and cholinergic (Chrm1) receptors. The role of MAOA in mediating prostate tumor growth/progression and tumor-nerve interactions in xenograft mouse models will be further discussed.

Conclusions: We demonstrated that MAOA and its associated neurotrophic and axon guidance genes induce PCa neuromimicry, and may serve as a driver promoting perineural PCa metastasis.

Impact: Our results will provide insights into understanding how PCa neuromimicry mediates PCa-nerve communications and also lay mechanistic foundations on developing rational strategies for improved treatment of PCa metastasis.

This work was supported by Department of Defense Prostate Cancer Research Program grant W81XWH-15-1-0493 (to B.J.W. and H.E.Z.). We thank Mr. Gary Mawyer for editorial assistance.

MAOA-Dependent Activation of Sonic Hedgehog-IL6-RANKL Signaling Network Promotes Prostate Cancer Metastasis by Engaging Tumor-Stromal Cell Interactions

Jason Boyang Wu[1,2,*], Lijuan Yin[1], Changhong Shi[1], Qinlong Li[1,3], Peng Duan[1], Jen-Ming Huang[1], Chunyan Liu[1], Fubo Wang[1,4], Michael Lewis[5], Yang Wang[6], Tzu-Ping Lin[7,8], Chin-Chen Pan[9], Edwin M. Posadas[1,10], Haiyen E. Zhau[1], and Leland W.K. Chung[1,*]

[1]Uro-Oncology Research Program, Samuel Oschin Comprehensive Cancer Institute, Department of Medicine, Cedars-Sinai Medical Center, Los Angeles, CA 90048, USA
[2]Department of Pharmaceutical Sciences, College of Pharmacy, Washington State University, Spokane, WA 99210, USA
[3]Department of Pathology, Xijing Hospital, the Fourth Military Medical University, Xi'an, Shaanxi 710032, China
[4]Department of Urology, Changhai Hospital, the Secondary Military Medical University, Shanghai 200433, China
[5]West Los Angeles VA Medical Center, Los Angeles, CA 90073, USA
[6]Department of Pathology, Changhai Hospital, the Secondary Military Medical University, Shanghai 200433, China
[7]Department of Urology, Taipei Veterans General Hospital, Taipei, Taiwan 11217, ROC
[8]Department of Urology, School of Medicine and Shu-Tien Urological Research Center, National Yang-Ming University, Taipei, Taiwan 11217, ROC
[9]Department of Pathology, Taipei Veterans General Hospital, Taipei, Taiwan 11217, ROC
[10]Division of Hematology/Oncology, Department of Medicine, Cedars-Sinai Medical Center, Los Angeles, CA 90048, USA

*Correspondence: Leland.Chung@cshs.org (L.W.C.) or boyang.wu@wsu.edu (J.B.W.)

Running Title: MAOA promotes prostate cancer metastasis

SUMMARY

Metastasis is a predominant cause of death for prostate cancer (PCa) patients; however, the underlying mechanisms are poorly understood. We report that monoamine oxidase A (MAOA) is a clinically and functionally important mediator of PCa bone and visceral metastases, activating paracrine Shh signaling in tumor-stromal interactions. MAOA provides tumor cell growth advantages in the bone microenvironment by stimulating IL6 release from osteoblasts, and triggers skeletal colonization by activating osteoclastogenesis through osteoblast production of RANKL and IL6. MAOA inhibitor treatment effectively reduces metastasis and prolongs mouse survival by disengaging the Shh-IL6-RANKL signaling network in stromal cells in the tumor microenvironment. These findings provide a rationale for targeting MAOA and its associated molecules to treat PCa metastasis.

Significance

Metastasis in advanced prostate cancer is a major clinical problem affecting quality of life and survival. Current therapies do not effectively limit disease progression and only moderately improve patient survival. The molecular and cellular events that initiate the metastatic niche and nurture metastases remain unclear. We show that elevated expression of MAOA activates the Shh-IL6-RANKL signaling network to promote tumor seeding and colonization to bone and visceral organs, creating a vicious cycle between cancer and stromal cells clinically associated with prostate cancer metastasis. MAOA inhibitors clinically used as antidepressants restrict metastasis and extend mouse survival, providing strong preclinical evidence for using MAOA inhibitors as therapeutic agents for prostate cancer metastasis.

INTRODUCTION

Advanced prostate cancer (PCa) is accompanied by the development of metastasis, particularly skeletal metastasis in up to 90% of patients dying from PCa, as confirmed at autopsy (Bubendorf et al., 2000). Bone metastasis and skeletal-related complications including bone pain, bone fracture, spinal cord compression, impaired mobility, infection, and hypercalcemia are the main cause of PCa death (Coleman, 2006). Therapeutic advances have been limited and most advanced disease remains incurable.

Bone metastases consist morphologically of aberrant osteolytic and osteoblastic components (Logothetis and Lin, 2005). PCa bone metastases are most often radiographically characterized as osteoblastic, but histologic evidence reveals a heterogeneous mixture of osteolytic and osteoblastic lesions (Berruti et al., 1996; Percival et al., 1987). The osteoblastic features are well-established, and a growing body of evidence shows the fundamental osteolytic component of PCa skeletal metastases (Keller and Brown, 2004; Sottnik and Keller, 2013). The bone resorption step preceding bone formation may be a prerequisite for tumor cell homing to bone and the nourishing tumor growth by pro-tumorigenic changes in the bone microenvironment (Yonou et al., 2004). Bone resorption is also needed for subsequent bone formation, since osteoblastic metastases are seen to form on trabecular bone at the sites of previous osteoclastic resorption (Carlin and Andriole, 2000; Charhon et al., 1983). This cascade of events suggests that an osteolysis-initiated overall increase in bone turnover and bone remodeling, coupling both osteoclastic and osteoblastic activities, drives osteoblastic PCa bone metastasis (Ibrahim et al., 2010; Keller and Brown, 2004; Sottnik and Keller, 2013).

Development and outgrowth of cancer cell bone lesions is largely regulated by intrinsic cellular and molecular interactions between PCa cells and stromal cells in the bone microenvironment (Keller and Brown, 2004; Morrissey and Vessella, 2007). Tumor cells stimulate osteoclastogenesis and osteoclast activity by altering the production of osteoblast-expressing proteins, including receptor activator of NFκB ligand (RANKL) and osteoprotegerin

(OPG), whose ratios determine the overall bone resorption, or secreting signaling molecules such as parathyroid hormone-related protein (PTHrP) to stimulate osteoblasts to produce more RANKL (Keller and Brown, 2004). The consequent bone destruction releases growth factors such as transforming growth factors β (TGFβs) and bone morphogenetic proteins (BMPs) from the mineralized bone matrix, further enhancing tumor growth and survival in a vicious cycle (Guise et al., 2006). Despite emerging molecular discoveries, a more comprehensive understanding of bone metastasis is needed to develop effective therapies.

Monoamine oxidase A (MAOA) is a mitochondria-bound enzyme that catalyzes the degradation of biogenic and dietary monoamines by oxidative deamination (Shih et al., 1999). We and others (True et al., 2006; Wu et al., 2014) have shown an association between increased MAOA expression, PCa progression and worse clinical outcomes. We also demonstrated that one of MAOA's key functions is to induce epithelial-mesenchymal transition (EMT) by producing excessive intracellular levels of hydrogen peroxide, a major reactive oxygen species byproduct generated by MAOA-mediated enzymatic reactions. EMT increases cancer cell aggressiveness, invasiveness and metastatic potential (Wu et al., 2014). MAOA is also involved in the pathology of depressive disorders (Campbell et al., 2012; Shih et al., 1999), and stress and depression have been shown to have neurohormonal effects via activation of the sympathetic nervous system on the host bone marrow stroma to promote breast cancer cell bone metastasis by inducing the expression of bone-tropic factors such as RANKL. Nevertheless, MAOA's function in PCa metastasis has not been fully addressed. This study focuses on the role of MAOA in PCa bone metastasis, which also sheds light on MAOA's role in visceral metastasis.

RESULTS

MAOA Expression Increases with PCa Metastasis

We examined MAOA expression in a spectrum normal prostate gland and primary and bone metastatic prostate tumor specimens, and found elevated MAOA expression in PCa bone metastases compared to normal and primary PCa epithelia (Figure 1A, Table S1). Two previously reported PCa clinical data sets showed higher *MAOA* mRNA levels in bone and visceral metastases compared to primary tumors (Figure 1B). We collected primary tumor and bone metastatic samples from PCa patients sequentially developing localized and metastatic disease, and demonstrated increased MAOA protein expression in bone metastases relative to primary tumors in 3 cases (Figure S1). We next assessed *MAOA* mRNA levels in 3 pairs of isogenic human PCa cell lines, C4-2B, $ARCaP_{BMC2}$ and PC-3M, metastasis-derived sublines of C4-2, $ARCaP_M$ and PC-3 cells respectively, with higher propensity for metastasis than their parental cells (Kozlowski et al., 1984; Thalmann et al., 1994; Zhang et al., 2010). *MAOA* mRNA levels were higher in C4-2B, $ARCaP_{BMC2}$ and PC-3M cells compared to their parental cells (Figure 1C). Increased *MAOA* mRNA expression was seen in C4-2, $ARCaP_M$ and PC-3M bone metastases in intracardiac models compared to both primary tumors and visceral metastases derived from orthotopic and intracardiac models respectively (Figure 1D). Taken together, these results strongly associate MAOA expression with PCa metastasis.

MAOA Mediates PCa Metastasis

To test whether MAOA promotes PCa metastasis, we stably overexpressed MAOA in PC-3 cells with low basal levels of MAOA (Figure 2A) (Wu et al., 2014) and subjected cells to stable labeling with luciferase (Figures S2A-S2C). Intracardiac injection of control PC-3 cells expressing an empty vector rapidly developed distant metastasis in mice, predominantly in bone. Overexpression of MAOA in PC-3 cells further accelerated the frequency of bone metastasis without affecting visceral metastasis (Table S2). Higher incidence (Figure 2B) and greater tumor burden (Figure 2C) were measured by weekly bioluminescence imaging (BLI) in mouse skeletons inoculated with MAOA-overexpressing cells compared to controls. At the experimental

endpoint mice were euthanized and circulating tumor cells (CTCs) from peripheral blood, defined as irregularly shaped CD45-negative and CK-positive nucleated cells, were counted as an indicator of the extent of PCa metastasis. The number of CTCs in blood increased over 7-fold in mice inoculated with MAOA-overexpressing cells 10 weeks after injection compared to controls (Figure 2D). We confirmed that BLI measurement of bone metastasis corresponded to the results from necropsy, X-ray and microCT analyses (Figure 2E). Mice harboring MAOA-overexpressing cells developed higher tumor burdens histologically (Figure 2F) and more severe osteolytic bone lesions radiographically (Figure 2G) than control mice. MicroCT showed reduced trabecular bone with a significant decrease in both relative bone volume and trabecular thickness in mice injected with MAOA-overexpressing cells compared to controls (Figures 2H and 2I). Histological analysis also showed a 2.4-fold increase in the number of tartrate-resistant acid phosphatase-positive ($TRAP^+$) osteoclasts relative to the bone surface area surrounded by MAOA-overexpressing tumor cells compared to controls (Figures 2E and 2J). Ki-67 staining of bone metastases revealed a 2-fold increase of proliferating tumor cells in mice with MAOA-overexpressing cells compared to controls (Figure 2K). We were able to recapitulate MAOA promotion of metastasis in another androgen-independent metastatic human PCa cell line, CWR22Rv1 (Figures S2D-S2J).

Next, we stably silenced MAOA expression by shRNA in several bone-metastatic human PCa cell lines. MAOA knockdown (KD) in C4-2 cells showing abundant expression of MAOA significantly delayed the onset of bone metastasis, reduced bone tumor burden, and extended mouse survival compared to control cells expressing scrambled shRNA (Figures 3A-3E). Two other highly bone-metastatic PCa cell lines with high MAOA expression, $ARCaP_M$ and PC-3M, showed similar results (Figures 3F-3O). Bone metastasis was more frequent than visceral metastases in control cells for all 3 human PCa cell lines, consistent with clinical observations (Table S2), confirmed by X-ray, microCT and histological analyses (Figures 3E, 3J and 3P). Quantitative analysis of bone regions and decalcified bone sections demonstrated that MAOA

KD in C4-2 cells significantly reduced the severity of osteolytic bone lesions, with less reduction of relative bone volume and trabecular thickness, and decreased the number of $TRAP^+$ osteoclasts along the bone-tumor interface compared to controls (Figures 3Q-3T). Ki-67 staining of bone metastases revealed a 47% decrease of $Ki\text{-}67^+$ cells in the MAOA-KD group compared to controls (Figure 3U). The other 2 human cell lines tested had similar results.

We also examined whether MAOA affects the osteoblastic features of bone metastases in our models, since C4-2 and $ARCaP_M$ cells exhibited mixed osteolytic/osteoblastic phenotypes in bone metastases (Odero-Marah et al., 2008; Wu et al., 1998). We found reduced osteocalcin expression, a marker of osteoblasts and the bone formation process, in MAOA-KD tumor-associated bone cells compared to controls, indicating a decreasing trend of osteoblast differentiation (Figures S3A-S3C). We also found prevalently reduced expression of a panel of markers of osteoblastic metastases, including OPG, PGK1, Substance P (TAC1) and EMID1 (Larson et al., 2013), in MAOA-KD bone metastases relative to controls (Figures S3D-S3F). These findings in aggregate indicate that MAOA promotes PCa metastasis and drives the development of osteoblastic lesions after initially promoting osteoclastic resorption.

MAOA Activates the Sonic Hedgehog (Shh) Pathway in PCa

Given that MAOA is mainly responsible for metabolizing monoamines (Shih et al., 1999), which is unlikely to be a mechanism directly mediating bone metastasis, we speculated that MAOA might function through downstream signaling molecules promoting tumor-bone cell interactions in a paracrine manner. Preliminary screening by a qPCR array assembling a panel of genes implicated in tumor-stromal interactions identified hedgehog (Hh) as the top candidate (Figure S4A). Hh signaling is triggered by binding one of 3 soluble Hh ligands (Sonic [Shh], Desert [Dhh] or Indian [Ihh]) to transmembrane protein Ptch1, which relieves the downstream depression of Smoothened (SMO) and activates Gli transcription factors, facilitating their translocation to the nucleus and induction of downstream gene expression (McMillan and

Matsui, 2012). Aberrantly activated Hh signaling pathways have been implicated in progression and metastasis, particularly bone metastasis, in a variety of cancers including PCa (Amakye et al., 2013; Sanchez et al., 2004; Alexaki et al., 2010; Cannonier et al., 2016).

We showed that *Shh* but not *Dhh* and *Ihh* mRNA expression was positively regulated by MAOA in 3 PCa cell lines (Figures 4A, S4B and S4C), as also demonstrated at the protein level in cell culture media and tumor xenograft bone metastases by ELISA and immunohistochemical (IHC) staining (Figures 4B and 4C). Genetic ablation of Shh significantly reduced MAOA-induced cell invasion and migration by 33% and 36% respectively (Figures 4D and 4E), indicating that Shh functionally mediated MAOA's effect on PCa cell behavior.

Given the regulation of *Shh* mRNA by MAOA at the transcriptional level, we explored the possible transcriptional machinery for MAOA activation of Shh. Examining the 1-kb *Shh* promoter sequence with the PROMO 3.0 search tool to predict putative transcription factor binding sites, and the literature on transcription factors implicated in PCa, we constructed a qPCR array to screen a panel of transcription factors in 2 pairs of isogenic MAOA-manipulated cell lines (Figure S4D). Combined with protein-level validation, this approach allowed us to identify Twist1, a basic helix-loop-helix transcription factor and master effector downstream of MAOA in PCa (Wu et al., 2014; Yang et al., 2004), as a top candidate transcription factor for *Shh* gene regulation. We showed that genetic silencing of *Twist1* significantly reduced MAOA-enhanced *Shh* expression at the mRNA and protein levels in PC-3 cells (Figures 4F-4H). We analyzed the 1-kb *Shh* promoter sequence and identified a Twist1-binding E-box site (-474/-469) (Figure 4I) (Yang et al., 2004). Searching for the consensus Twist1-binding E-box and its surrounding sequences in *Shh* promoter across species, we found that this E-box (CAGGTG) is highly conserved among the amniotic genomes examined (Figure 4J). We generated a *Shh* promoter reporter construct with a mutant E-box which was no longer induced by both overexpression of Twist1 and MAOA unlike its wild-type (WT) counterpart (Figures 4K and 4L). We also conducted chromatin immunoprecipitation (ChIP) assays to confirm direct occupancy of

Twist1 with this E-box in *Shh* promoter. Natural *Shh* promoter showed a 41% higher association of endogenous Twist1 protein with the E-box by MAOA overexpression compared to controls, and this association was reduced by 57% after Twist1 KD (Figure 4M). IHC analysis further revealed significant co-expression correlations between MAOA and Shh, Twist1 and Shh, and MAOA and Twist1 in a clinical cohort of PCa bone metastases, as clinical evidence of MAOA/Twist1-mediated regulation of Shh (Figure 4N, Table S3). These results in sum demonstrate that MAOA induces the Shh pathway through the downstream effector Twist1 which directly interacts with an E-box site in *Shh* promoter in PCa cells.

MAOA Confers PCa Cell Growth Advantages by Activating Shh Signaling in Osteoblasts

MAOA significantly promoted bone metastasis in mice by altering osteoclast and osteoblast activity (Figures 3, S3) allowing the bone microenvironment to support cancer cell homing, growth and survival via osteoclastic and osteoblastic reactions such as the release of osteoblast-produced factors (Weilbaecher et al., 2011). Thus, we hypothesized that MAOA-mediated cell signaling may facilitate communications between tumor cells and the bone microenvironment where tumor-derived Shh plays a paracrine mediating role, and investigated the involvement of supporting osteoblasts and osteoclasts in MAOA/Shh-mediated bone metastasis in an in vitro co-culture system.

First, we tested whether tumor MAOA activated Shh signaling in associated osteoblasts using mouse MC3T3-E1 cells, verified by demonstrating both differentiation and mineral production after induction (Figures S5A-S5C). Co-culturing MC3T3-E1 osteoblasts expressing a *Gli* reporter with C4-2 cells, we observed a 46% decrease of Gli activity in osteoblasts where tumor MAOA expression was silenced compared to controls. This decrease was abolished by cyclopamine, an inhibitor of SMO that blocks Shh signaling and Gli activity (Figure 5A). Consistent results were obtained for testing Gli reporter activity in osteoblasts co-cultured with MAOA-overexpressing PC-3 cells (Figure S6A). Osteoblasts separated from co-cultured MAOA-

KD cells relative to control cells showed reduced expression of several Shh target genes, unlike cyclopamine-treated co-cultures (Figure 5B), which were confirmed in two other co-cultures with PC-3 and ARCaP$_M$ tumor cells (Figures S6B, S6C). Genetic ablation of tumor MAOA in co-culture also downregulated osteoblast expression of select *TGFβs* and *BMP*s (Figure 5C), important for bone metastasis formation and signaling crosstalk with the Shh pathway (Hurchla and Weilbaecher, 2012).

To investigate whether osteoblasts contribute to elevated tumor proliferation, we co-cultured C4-2 cells dual-labeled with red fluorescence protein (RFP) and luciferase over a monolayer of MC3T3-E1 osteoblasts to quantify tumor cell proliferation by fluorescence readout and luciferase assay. MAOA-KD tumor cells formed RFP$^+$ colonies 42% smaller in diameter compared to controls (Figures 5D, 5E), paralleling a 42% decrease in the number of MAOA-KD tumor cells relative to controls (Figure 5F). Cyclopamine treatment abolished the growth disadvantages of MAOA-silenced tumor cells in co-culture, showing that paracrine Shh signaling maintains tumor cell growth in co-culture (Figures 5E, 5F, S6D). C4-2 cells directly treated with different co-culture conditioned media confirmed these results (Figure S6E). Genetic inhibition of Shh signaling in MC3T3-E1 osteoblasts via siRNA-mediated silencing of *Gli1* or *Gli2*, two indispensable transcription factors of the Shh pathway, similarly blunted the growth disadvantages of MAOA-KD tumor cells in co-culture (Figure 5G). In addition, we found that treating MC3T3-E1 cells with MAOA-KD C4-2 cell conditioned media reduced osteoblast differentiation and calcium production compared to control media, which was diminished by cyclopamine treatment (Figures S5D-S5F). Direct Shh treatment of osteoblasts had similar results (Figures S5G-S5I).

Notably, tumor MAOA KD elicited a more robust decrease in tumor cell proliferation in co-culture than single tumor cell culture (Figure 5F), suggesting the potential involvement of tumor MAOA-responsive gene(s) in osteoblasts in MAOA-dependent tumor cell growth. A qPCR-coupled genomic search identified interleukin 6 (IL6) as a required paracrine mediator of MAOA

signaling in osteoblasts for regulating tumor cell growth. IL6 has been implicated in bone metastasis (Shariat et al., 2001) and associated with poor clinical outcomes (Nakashima et al., 2000). Compared with MC3T3-E1 osteoblasts cultured alone, *IL6* mRNA expression was significantly induced 3.6-fold in co-culture with control C4-2 cells, which was downregulated by 39% in the presence of co-cultured MAOA-KD C4-2 cells. These differences were abolished by cyclopamine treatment (Figures 5H, S6F). Similar observations at the IL6 protein level by ELISA (Figure 5I) also depended on MAOA activation of the paracrine Shh pathway (Figures 5I, 5J).

To test whether MAOA/Shh signaling modulates *IL6* gene expression at the transcriptional level, we transfected an *IL6* promoter reporter construct into osteoblasts and measured activity in co-cultures with PC-3 cells. *IL6* promoter activity increased by 78% in co-culture with MAOA-overexpressing tumor cells, which decreased by 33% with tumor Shh silencing (Figure 5K). Next we determined whether Gli transcription factors are involved in *IL6* regulation. We analyzed the 1.3-kb *IL6* promoter sequence and located a consensus Gli-binding site (-750/-742) with a core sequence (CACCC) identical to the canonical one (Figure 5L) (Kinzler and Vogelstein, 1990). To test its functionality, we generated an *IL6* promoter reporter mutant construct and showed that it was no longer induced in osteoblasts by Shh treatment compared to WT counterparts (Figure 5M). ChIP assays in osteoblasts treated with conditioned media from MAOA/Shh-manipulated PC-3 cells demonstrated significantly increased occupancy of Gli1 and Gli2 proteins at the Gli-binding element of *IL6* promoter in osteoblasts treated with conditioned media of MAOA-overexpressing tumor cells relative to controls, which was abolished by treatment with conditioned media from MAOA-overexpressing/Shh-KD tumor cells (Figure 5N).

Finally, we tested whether osteoblast secretion of IL6 is required to maintain tumor cell proliferation in co-culture. Inhibition of IL6 by a neutralizing antibody minimized the effect of MAOA on tumor cell growth in osteoblast co-cultures (Figure 5O) while treatment of control tumor cells with recombinant IL6 protein significantly enhanced cell proliferation (Figure 5P).

These results revealed a feed-forward loop where tumor MAOA/Shh signaling stimulates the release of IL6 from osteoblasts via transcriptional activation of IL6 by direct binding of Gli1/Gli2 to *IL6* promoter to induce tumor cell proliferation.

MAOA Promotes Osteoclast Differentiation by Shh Signaling-Mediated Activation of Osteoblast-Derived RANKL and IL6

Because MAOA-overexpressing tumor cells provoked an osteolytic phenotype in mouse skeletal metastases (Figures 2, 3), we investigated the impact of tumor MAOA on osteoclastogenesis via osteoblast activation to produce soluble factors in mouse pre-osteoclast RAW 264.7 cells with verified ability to differentiate and form pits by RANKL induction (Figure S7A, S7B). When RAW 264.7 cells were treated with conditioned media from co-culture of MC3T3-E1 osteoblasts with MAOA-KD tumor cells, osteoclastogenesis as measured by $TRAP^+$ osteoclast number decreased up to 65% compared to controls (Figures 6A, 6B). $TRAP^+$ osteoclasts treated by MAOA-KD co-culture conditioned media were significantly smaller, by up to 39% in diameter compared to those induced by control media (Figure 6C). The reduced osteoclast differentiation caused by MAOA-KD co-culture media was abolished when cyclopamine-treated co-culture media were used, suggesting that the paracrine Shh signaling by which tumor cells communicate with osteoblasts is obligatory for MAOA to affect osteoclast differentiation (Figures 6A-6C). Mouse *Trap* mRNA expression was consistently reduced up to 52% in osteoclasts nourished with MAOA-KD co-culture media compared to control media. This decrease was blunted when osteoclasts were grown in cyclopamine-treated co-culture media (Figure 6D). When we profiled mRNA expression of select markers for osteoclast differentiation in RAW 264.7 cells treated with different co-culture media, the expression of most markers was downregulated in osteoclasts treated with MAOA-KD co-culture media compared to controls, and further suppressed by cyclopamine-treated co-culture media (Figure 6E).

Osteolytic bone metastasis is largely mediated by altered expression of RANKL and OPG causing an imbalance favorable to bone destruction. Osteoclastogenesis can be regulated by non-canonical pathways in which IL6, CSF-1 and TNFα substitute for RANKL to promote osteoclast differentiation and bone resorption in a RANKL-independent manner (Hemingway et al., 2011; Keller and Brown, 2004). ELISA showed that osteoblast-derived RANKL secretion was significantly reduced in co-cultures of MC3T3-E1 osteoblasts with MAOA-KD tumor cells relative to controls, which was reversed by cyclopamine treatment (Figure 6F). We next determined whether upregulation of RANKL and IL6 in osteoblasts contributed to MAOA's effect on osteoclast differentiation. Conditioned media from co-cultures combining osteoblasts with MAOA-overexpressing PC-3 cells produced a 3.6-fold increase in the number of mature osteoclasts in RAW264.7 cells, counted as $TRAP^+$ multinucleated cells, compared to control media, which was reversed by MAOA-KD co-culture conditioned media. Conditioned media containing a neutralizing antibody against RANKL also decreased MAOA-induced osteoclastogenesis by 65%, and inhibition was further enhanced by adding IL6 antibody, restoring osteoclast maturation to MAOA KD levels (Figure 6G). These findings demonstrate that tumor MAOA induces osteoblast production of RANKL and IL6 by paracrine Shh signaling to achieve a MAOA-driven osteolytic phenotype in mouse skeleton.

Pharmacological MAOA Inhibition Reduces Metastasis by Disrupting the Shh-IL6-RANKL Signaling Network in the Tumor Microenvironment

To test whether a MAOA inhibitor could reduce metastasis, mice were inoculated intracardially with $ARCaP_M$ cells and treated with clorgyline, a potent irreversible MAOA inhibitor, 18 days after tumor inoculation. Before therapeutic intervention, mice developed multiple metastases in hind limbs and jaws as examined by BLI, parallel to slight visible osteolytic lesions measured by X-ray in some mice. Clorgyline treatment led to a roughly 9-day delay in bone metastasis onset (Figure 7A) and a 5.8-fold decrease in bone metastasis burden by BLI (Figures 7B and 7D).

Importantly, the survival of clorgyline-treated mice significantly improved, with an 83% drop in mortality compared to control mice over an 8-week period (Figure 7C). Quantitative microCT analysis of femoral and tibial bone lesions showed less reduction in relative bone volume and trabecular thickness in clorgyline-treated mice than controls (Figures 7E, 7G, 7H), consistent with fewer X-ray lesion areas in clorgyline-treated mice relative to controls (Figures 7D, 7F). Histological analysis demonstrated 55% fewer $TRAP^+$ osteoclasts in bone metastases in clorgyline-treated mice (Figures 7E, 7I), indicating reduced osteoclast activity. Clorgyline treatment also led to a 53% decrease of $Ki\text{-}67^+$ tumor cells in bone metastases (Figure 7J). Clorgyline did not interfere with osteoclast and osteoblast activities when cultured alone in vitro (Figure S7). In addition, clorgyline-treated bone metastases showed reduced differentiation of tumor-associated osteoblasts and osteoblastic characteristics of bone metastases by decreased expression of osteocalcin and a panel of osteoblastic metastasis markers compared to controls (Figure S3G-S3L).

Clorgyline treatment also downregulated Shh signaling in tumor-surrounding bone stromal cells, evidenced by reduced expression of select Shh target genes (*Ptch1*, *Gli1* and *Hhip1*) and Shh-interacting partner genes (*TGFβ1*, *BMP2* and *BMP4*) compared to controls. After clorgyline treatment, *RANKL* and *IL6* mRNA expression in mouse bone stromal cells was reduced by 46% and 40%, respectively (Figure 7K). Finally, we explored MAOA/Shh-mediated signaling in tumor-bone cell interactions in the clinical setting, and found significant co-expression correlations between tumor-expressed MAOA/Shh/Twist1 and stroma-derived IL6/Gli1/Gli2, providing strong clinical evidence for the critical role of the MAOA/Shh-mediated pathway in bone metastasis (Figures 7L, 7M, Table S3).

In summary, our preclinical studies reveal a tumor MAOA-mediated vicious cycle among tumor cells, osteoblasts, osteoclasts and stromal cells facilitating PCa metastasis to bone and visceral organs, which was effectively reduced by pharmacological MAOA inhibition disengaging the Shh-IL6-RANKL signaling network in the tumor microenvironment.

DISCUSSION

This study showed that elevated MAOA expression in PCa cells promotes metastasis, including bone metastasis by activating paracrine Shh signaling to mediate tumor-bone cell interactions (Figure 7N). Upregulation of MAOA could be under the synergistic control of aberrant oncogenic (activation of c-Myc and loss of PTEN and p53) and androgenic signaling (Wu et al., 2014). Although not a major emphasis in this study, we demonstrated that MAOA enhances PCa visceral metastasis in a cell context-dependent manner. Hence, MAOA upregulation and promotion of metastasis is associated with most sites of PCa metastasis rather than bone-specific.

Our findings identify the initiation of PCa bone metastasis via a MAOA/Shh-induced osteolytic reaction in the tumor-bone interface, with active participation of osteoblasts, as evidenced by a positive relationship between tumor MAOA expression and osteoblast differentiation and mineralization, dependent on paracrine Shh signaling. The coupling of bone resorption and new bone formation mediated by MAOA/Shh signaling suggests dual roles of MAOA directing PCa cell interactions with osteoclasts and osteoblasts to enhance overall bone turnover and bone remodeling.

Emerging evidence suggests that developmental signaling pathways activated in a paracrine manner between tumor and stromal cells facilitate cancer progression (Sethi and Kang, 2011). Several previous studies reported aberrant Notch signaling pathway activation in PCa metastasis, recurrence and chemoresistance (Santagata et al., 2004). We demonstrated that MAOA activates the Shh pathway through direct interaction of Twist1 with *Shh* promoter, consistent with the molecular regulation of limb bud development where disrupted expression of Shh signaling-associated genes (e.g. *Shh*, *Ptch*, *Gli1* and *Gli2*) was found in *Twist1*$^{-/-}$ forelimb buds (O'Rourke et al., 2002). Interestingly, while the Shh signaling pathway is critical for prostate development (Podlasek et al., 1999) and for growth of advanced PCa (Sanchez et al.,

2004), Shh pathway activation alone has minimal growth-stimulating effects on PCa cells (Shigemura et al., 2011). In the context of tumor-stromal interactions, however, Shh-overexpressing prostate tumor xenografts showed accelerated growth rates in mice (Fan et al., 2004). Our results support these contrasting observations where activated Shh signaling promoted the growth of tumor cells co-cultured with osteoblasts compared to tumor cells cultured alone. These studies suggest that stroma-dependent Shh signaling between tumor and bone cells appears to promote PCa bone metastasis.

Numerous studies have demonstrated induced osteoclastogenesis by both RANKL-mediated canonical and RANKL-independent non-canonical pathways, with the latter involving RANKL substitutes such as IL6, TNFα and CSF-1 (Hemingway et al., 2011; Ishimi et al., 1990; Keller and Brown, 2004). IL6 promotes osteoclast differentiation primarily by inducing osteoclastic precursors, rather than inducing RANKL directly (Keller and Brown, 2004). These osteolytic factors may induce bone resorption alone or in concert (Hemingway et al., 2011; Ishimi et al., 1990). We demonstrated that MAOA activated osteoblast production of both RANKL and IL6, dependent on paracrine Shh signaling. MAOA inhibition reduced the expression of these genes in tumor-invading bone stromal cells. Thus inhibition of MAOA may target multiple molecules and associated pathways, with a broader inhibitory effect on bone metastasis than monotherapies like RANKL inhibition.

The small molecule inhibitor clorgyline, which inhibits MAOA enzymatic activity, showed promise in xenograft mouse models, disrupting the Shh-IL6-RANKL signaling network in bone stromal cells. The prevalent upregulation of MAOA in PCa bone and visceral metastases provides a rationale for using MAOA inhibitors to treat PCa metastasis. MAOA inhibitors are used clinically as antidepressants (Shih et al., 1999), and their effects on tumor growth, progression, and metastasis are still under investigation. The effectiveness of MAOA inhibitors for impeding PCa growth has been documented in tumor xenograft models (Flamand et al., 2010; Wu et al., 2014). Our observation that MAOA inhibitors suppressed EMT in tumor

xenografts suggests their use for treating metastasis (Wu et al., 2014). In this study MAOA inhibitor treatment effectively restricted PCa metastasis and prolonged mouse survival. However, MAOA inhibitors were reported to promote EMT in breast cancer cells (Satram-Maharaj et al., 2014). These controversial results suggest that the role of MAOA-associated signaling networks during cancer progression may be context-dependent.

In conclusion, we demonstrated the functional importance of MAOA for initiating the pre-metastatic niche in stromal cells and promoting PCa metastasis to bone and visceral organs, mediated by activation of paracrine Shh-IL6-RANKL signaling underlying tumor-stromal interactions. We also provide strong preclinical evidence for using MAOA inhibitors to disengage the Shh-IL6-RANKL interactive signaling network and disrupt tumor-stromal communication as a PCa metastasis therapy.

EXPERIMENTAL PROCEDURES

Clinical Specimens

The IRBs of all institutions involved in this study reviewed and approved all human studies. Two PCa tissue microarrays composed of 74 primary adenocarcinomas, without neuroendocrine carcinomas as verified by a pathologist, were obtained from Imgenex and US Biomax. Additional archival normal prostate and PCa bone metastatic specimens were obtained from our institutions. IHC analysis of MAOA expression in TMA and clinical samples and the expression of other markers in the clinical cohort of bone metastatic samples is described in the Supplemental Experimental Procedures.

Animal Studies

All animal studies received prior approval from the Cedars-Sinai Medical Center IACUC and complied with IACUC recommendations. Male 4- to 6-week-old athymic nude mice, SCID, SCID-beige mice, and C57BL/6 mice were purchased from Taconic. For metastasis studies, 1 ×

10^6 luciferase-tagged tumor cells were injected into the left cardiac ventricle of anesthetized mice as described previously (Xu et al., 2006). Metastasis development was monitored by BLI with a Xenogen IVIS Spectrum Imaging System (PerkinElmer) as described previously (Wu et al., 2014). Living Image software analysis (PerkinElmer) measured photon flux in mouse limbs. BLI signal data were acquired after background subtraction. Bone metastasis-free curves represent the time point at which each mouse developed bone metastasis by threshold BLI signals in limbs.

To determine the therapeutic effect of clorgyline on metastasis, 1×10^6 luciferase-tagged $ARCaP_M$ cells were injected into anesthetized SCID-beige mice intracardially. Mice were randomly assigned to 2 groups (clorgyline vs. vehicle, n=9 for each) for treatment based on BLI signals in limbs 18 days after tumor injection. Daily i.p. injection of clorgyline (30 mg/kg) was given for up to 6 weeks, with saline injection for the control group. Development of metastasis was monitored by BLI.

Biochemical Analyses

Total RNA was isolated using an RNeasy Mini Kit (Qiagen) and reverse-transcribed to cDNA by M-MLV reverse transcriptase (Promega) following the manufacturer's instructions. Details on primers and methods used for qPCR are provided in the Supplemental Experimental Procedures. Total RNA from formalin-fixed paraffin-embedded tissue sections was isolated by an RNeasy FFPE Kit (Qiagen) following the manufacturer's instructions. For Western blot, cells were extracted with radioimmunoprecipitation assay buffer in the presence of a protease and phosphatase inhibitor cocktail (Thermo Scientific), and blots were performed as described previously (Wu et al., 2014) using primary antibodies against MAOA (H-70, Santa Cruz), Shh (C9C5, Cell Signaling), Twist1 (Twist2C1a, Santa Cruz) or β-Actin (AC-15, Santa Cruz). Human Shh and mouse IL6 and RANKL protein secretion in cell culture media were quantified by

species-specific ELISA from RayBiotech and Peprotech respectively by the manufacturer's protocols.

Statistical Analysis

Data are presented as the mean ± SEM as indicated in figure legends. Comparisons between Kaplan-Meier curves were performed using the long-rank test. Correlations were determined by Pearson correlation. All other comparisons were analyzed by unpaired 2-tailed Student's t test. A p value < 0.05 was considered statistically significant.

SUPPLEMENTAL INFORMATION

Supplemental Information: 7 Supplemental Figures, 3 Supplemental Tables, Supplemental Experimental Procedures, and Supplemental References.

AUTHOR CONTRIBUTIONS

Conceptualization, J.B.W. and L.W.C.; Methodology, J.B.W. and L.Y.; Investigation, J.B.W., L.Y., C.S., Q.L., P.D., J.H., and C.L.; Resources, F.W., M.L., Y.W., T.L., C.P., E.M.P, and H.E.Z.; Writing – Original Draft, J.B.W. and L.W.C.; Writing – Review & Editing, J.B.W. and L.W.C.; Supervision: J.B.W. and L.W.C.; Funding Acquisition: J.B.W. and L.W.C.

ACKNOWLEDGEMENTS

This work was supported by NIH/NCI grant 2P01CA098912, the Board of Governors Cancer Research Chair and the Steven Spielberg Fund in Prostate Cancer Research (to L.W.K. Chung), and US Department of Defense PCRP grant W81XWH-15-1-0493 (to J.B. Wu). We thank Gary Mawyer for editorial assistance.

REFERENCES

Alexaki, V. I., Javelaud, D., Van Kempen, L. C., Mohammad, K. S., Dennler, S., Luciani, F., Hoek, K. S., Juarez, P., Goydos, J. S., Fournier, P. J.*, et al.* (2010). GLI2-mediated melanoma invasion and metastasis. J. Natl. Cancer Inst. *102*, 1148-1159.

Amakye, D., Jagani, Z., and Dorsch, M. (2013). Unraveling the therapeutic potential of the Hedgehog pathway in cancer. Nat. Med. *19*, 1410-1422.

Berruti, A., Piovesan, A., Torta, M., Raucci, C. A., Gorzegno, G., Paccotti, P., Dogliotti, L., and Angeli, A. (1996). Biochemical evaluation of bone turnover in cancer patients with bone metastases: relationship with radiograph appearances and disease extension. Br. J. Cancer *73*, 1581-1587.

Bubendorf, L., Schopfer, A., Wagner, U., Sauter, G., Moch, H., Willi, N., Gasser, T. C., and Mihatsch, M. J. (2000). Metastatic patterns of prostate cancer: an autopsy study of 1,589 patients. Hum. Pathol. *31*, 578-583.

Campbell, J. P., Karolak, M. R., Ma, Y., Perrien, D. S., Masood-Campbell, S. K., Penner, N. L., Munoz, S. A., Zijlstra, A., Yang, X., Sterling, J. A., and Elefteriou, F. (2012). Stimulation of host bone marrow stromal cells by sympathetic nerves promotes breast cancer bone metastasis in mice. PLoS Biol. *10*, e1001363.

Cannonier, S. A., Gonzales, C. B., Ely, K., Guelcher, S. A., and Sterling, J. A. (2016). Hedgehog and TGFbeta signaling converge on Gli2 to control bony invasion and bone destruction in oral squamous cell carcinoma. Oncotarget.

Carlin, B. I., and Andriole, G. L. (2000). The natural history, skeletal complications, and management of bone metastases in patients with prostate carcinoma. Cancer *88*, 2989-2994.

Charhon, S. A., Chapuy, M. C., Delvin, E. E., Valentin-Opran, A., Edouard, C. M., and Meunier, P. J. (1983). Histomorphometric analysis of sclerotic bone metastases from prostatic carcinoma special reference to osteomalacia. Cancer *51*, 918-924.

Coleman, R. E. (2006). Clinical features of metastatic bone disease and risk of skeletal morbidity. Clin. Cancer Res. *12*, 6243s-6249s.

Fan, L., Pepicelli, C. V., Dibble, C. C., Catbagan, W., Zarycki, J. L., Laciak, R., Gipp, J., Shaw, A., Lamm, M. L., Munoz, A.*, et al.* (2004). Hedgehog signaling promotes prostate xenograft tumor growth. Endocrinology *145*, 3961-3970.

Flamand, V., Zhao, H., and Peehl, D. M. (2010). Targeting monoamine oxidase A in advanced prostate cancer. J. Cancer Res. Clin. Oncol. *136*, 1761-1771.

Guise, T. A., Mohammad, K. S., Clines, G., Stebbins, E. G., Wong, D. H., Higgins, L. S., Vessella, R., Corey, E., Padalecki, S., Suva, L., and Chirgwin, J. M. (2006). Basic mechanisms responsible for osteolytic and osteoblastic bone metastases. Clin. Cancer Res. *12*, 6213s-6216s.

Hemingway, F., Taylor, R., Knowles, H. J., and Athanasou, N. A. (2011). RANKL-independent human osteoclast formation with APRIL, BAFF, NGF, IGF I and IGF II. Bone *48*, 938-944.

Hurchla, M. A., and Weilbaecher, K. N. (2012). Hedgehog-targeted therapeutics uncouple the vicious cycle of bone metastasis. Oncoimmunology *1*, 1411-1413.

Ibrahim, T., Flamini, E., Mercatali, L., Sacanna, E., Serra, P., and Amadori, D. (2010). Pathogenesis of osteoblastic bone metastases from prostate cancer. Cancer *116*, 1406-1418.

Ishimi, Y., Miyaura, C., Jin, C. H., Akatsu, T., Abe, E., Nakamura, Y., Yamaguchi, A., Yoshiki, S., Matsuda, T., Hirano, T., and et al. (1990). IL-6 is produced by osteoblasts and induces bone resorption. J. Immunol. *145*, 3297-3303.

Keller, E. T., and Brown, J. (2004). Prostate cancer bone metastases promote both osteolytic and osteoblastic activity. J. Cell. Biochem. *91*, 718-729.

Kinzler, K. W., and Vogelstein, B. (1990). The GLI gene encodes a nuclear protein which binds specific sequences in the human genome. Mol. Cell. Biol. *10*, 634-642.

Kozlowski, J. M., Fidler, I. J., Campbell, D., Xu, Z. L., Kaighn, M. E., and Hart, I. R. (1984). Metastatic behavior of human tumor cell lines grown in the nude mouse. Cancer Res. *44*, 3522-3529.

Larson, S. R., Zhang, X., Dumpit, R., Coleman, I., Lakely, B., Roudier, M., Higano, C. S., True, L. D., Lange, P. H., Montgomery, B.*, et al.* (2013). Characterization of osteoblastic and osteolytic proteins in prostate cancer bone metastases. Prostate *73*, 932-940.

Logothetis, C. J., and Lin, S. H. (2005). Osteoblasts in prostate cancer metastasis to bone. Nat. Rev. Cancer *5*, 21-28.

McMillan, R., and Matsui, W. (2012). Molecular pathways: the hedgehog signaling pathway in cancer. Clin. Cancer Res. *18*, 4883-4888.

Morrissey, C., and Vessella, R. L. (2007). The role of tumor microenvironment in prostate cancer bone metastasis. J. Cell. Biochem. *101*, 873-886.

Nakashima, J., Tachibana, M., Horiguchi, Y., Oya, M., Ohigashi, T., Asakura, H., and Murai, M. (2000). Serum interleukin 6 as a prognostic factor in patients with prostate cancer. Clin. Cancer Res. *6*, 2702-2706.

O'Rourke, M. P., Soo, K., Behringer, R. R., Hui, C. C., and Tam, P. P. (2002). Twist plays an essential role in FGF and SHH signal transduction during mouse limb development. Dev. Biol. *248*, 143-156.

Odero-Marah, V. A., Wang, R., Chu, G., Zayzafoon, M., Xu, J., Shi, C., Marshall, F. F., Zhau, H. E., and Chung, L. W. (2008). Receptor activator of NF-kappaB Ligand (RANKL) expression is associated with epithelial to mesenchymal transition in human prostate cancer cells. Cell Res. *18*, 858-870.

Percival, R. C., Urwin, G. H., Harris, S., Yates, A. J., Williams, J. L., Beneton, M., and Kanis, J. A. (1987). Biochemical and histological evidence that carcinoma of the prostate is associated with increased bone resorption. Eur. J. Surg. Oncol. *13*, 41-49.

Podlasek, C. A., Barnett, D. H., Clemens, J. Q., Bak, P. M., and Bushman, W. (1999). Prostate development requires Sonic hedgehog expressed by the urogenital sinus epithelium. Dev. Biol. *209*, 28-39.

Sanchez, P., Hernandez, A. M., Stecca, B., Kahler, A. J., DeGueme, A. M., Barrett, A., Beyna, M., Datta, M. W., Datta, S., and Ruiz i Altaba, A. (2004). Inhibition of prostate cancer proliferation by interference with SONIC HEDGEHOG-GLI1 signaling. Proc. Natl. Acad. Sci. USA *101*, 12561-12566.

Santagata, S., Demichelis, F., Riva, A., Varambally, S., Hofer, M. D., Kutok, J. L., Kim, R., Tang, J., Montie, J. E., Chinnaiyan, A. M*., et al.* (2004). JAGGED1 expression is associated with prostate cancer metastasis and recurrence. Cancer Res. *64*, 6854-6857.

Satram-Maharaj, T., Nyarko, J. N., Kuski, K., Fehr, K., Pennington, P. R., Truitt, L., Freywald, A., Lukong, K. E., Anderson, D. H., and Mousseau, D. D. (2014). The monoamine oxidase-A inhibitor clorgyline promotes a mesenchymal-to-epithelial transition in the MDA-MB-231 breast cancer cell line. Cell. Signal. *26*, 2621-2632.

Sethi, N., and Kang, Y. (2011). Dysregulation of developmental pathways in bone metastasis. Bone *48*, 16-22.

Shariat, S. F., Andrews, B., Kattan, M. W., Kim, J., Wheeler, T. M., and Slawin, K. M. (2001). Plasma levels of interleukin-6 and its soluble receptor are associated with prostate cancer progression and metastasis. Urology *58*, 1008-1015.

Shigemura, K., Huang, W. C., Li, X., Zhau, H. E., Zhu, G., Gotoh, A., Fujisawa, M., Xie, J., Marshall, F. F., and Chung, L. W. (2011). Active sonic hedgehog signaling between androgen independent human prostate cancer cells and normal/benign but not cancer-associated prostate stromal cells. Prostate *71*, 1711-1722.

Shih, J. C., Chen, K., and Ridd, M. J. (1999). Monoamine oxidase: from genes to behavior. Annu. Rev. Neurosci. *22*, 197-217.

Sottnik, J. L., and Keller, E. T. (2013). Understanding and targeting osteoclastic activity in prostate cancer bone metastases. Curr. Mol. Med. *13*, 626-639.

Thalmann, G. N., Anezinis, P. E., Chang, S. M., Zhau, H. E., Kim, E. E., Hopwood, V. L., Pathak, S., von Eschenbach, A. C., and Chung, L. W. (1994). Androgen-independent cancer progression and bone metastasis in the LNCaP model of human prostate cancer. Cancer Res. *54*, 2577-2581.

True, L., Coleman, I., Hawley, S., Huang, C. Y., Gifford, D., Coleman, R., Beer, T. M., Gelmann, E., Datta, M., Mostaghel, E*., et al.* (2006). A molecular correlate to the Gleason grading system for prostate adenocarcinoma. Proc. Natl. Acad. Sci. USA *103*, 10991-10996.

Weilbaecher, K. N., Guise, T. A., and McCauley, L. K. (2011). Cancer to bone: a fatal attraction. Nat. Rev. Cancer *11*, 411-425.

Wu, J. B., Shao, C., Li, X., Li, Q., Hu, P., Shi, C., Li, Y., Chen, Y. T., Yin, F., Liao, C. P*., et al.* (2014). Monoamine oxidase A mediates prostate tumorigenesis and cancer metastasis. J. Clin. Invest. *124*, 2891-2908.

Wu, T. T., Sikes, R. A., Cui, Q., Thalmann, G. N., Kao, C., Murphy, C. F., Yang, H., Zhau, H. E., Balian, G., and Chung, L. W. (1998). Establishing human prostate cancer cell xenografts in bone: induction of osteoblastic reaction by prostate-specific antigen-producing tumors in athymic and SCID/bg mice using LNCaP and lineage-derived metastatic sublines. Int. J. Cancer *77*, 887-894.

Xu, J., Wang, R., Xie, Z. H., Odero-Marah, V., Pathak, S., Multani, A., Chung, L. W., and Zhau, H. E. (2006). Prostate cancer metastasis: role of the host microenvironment in promoting epithelial to mesenchymal transition and increased bone and adrenal gland metastasis. Prostate *66*, 1664-1673.

Yang, J., Mani, S. A., Donaher, J. L., Ramaswamy, S., Itzykson, R. A., Come, C., Savagner, P., Gitelman, I., Richardson, A., and Weinberg, R. A. (2004). Twist, a master regulator of morphogenesis, plays an essential role in tumor metastasis. Cell *117*, 927-939.

Yonou, H., Ochiai, A., Goya, M., Kanomata, N., Hokama, S., Morozumi, M., Sugaya, K., Hatano, T., and Ogawa, Y. (2004). Intraosseous growth of human prostate cancer in implanted adult human bone: relationship of prostate cancer cells to osteoclasts in osteoblastic metastatic lesions. Prostate *58*, 406-413.

Zhang, S., Zhau, H. E., Osunkoya, A. O., Iqbal, S., Yang, X., Fan, S., Chen, Z., Wang, R., Marshall, F. F., Chung, L. W., and Wu, D. (2010). Vascular endothelial growth factor regulates myeloid cell leukemia-1 expression through neuropilin-1-dependent activation of c-MET signaling in human prostate cancer cells. Mol. Cancer *9*, 9.

FIGURE LEGENDS

Figure 1. MAOA Expression Is Associated with High PCa Metastasis Risk.
(A) Quantitative IHC analysis of MAOA protein expression in normal prostate (n=21), primary (n=74) and bone metastatic (Met, n=20) PCa clinical samples. Arrows indicate tumor areas. Scale bars: 20 μm. (B) *MAOA* mRNA levels (log2 intensity) in primary and metastatic (Met) PCa data set samples. (C) *MAOA* mRNA levels in 3 pairs of lineage-related human PCa cell lines by RT-qPCR. (D) *MAOA* mRNA levels in xenograft samples harvested from primary prostate tumors and bone/visceral metastases developed in orthotopic and intracardiac models respectively by RT-qPCR. Data represent the mean ± SEM. *p<0.05, **p<0.01. ns, not significant. See also Figure S1 and Table S1.

Figure 2. Enforced MAOA Expression Promotes PCa Metastasis.
(A) Western blotting analysis of MAOA protein levels in control (Vector) and MAOA-overexpressing (MAOA) PC-3 cells. (B) Kaplan-Meier bone metastasis-free curve of mice inoculated with indicated PC-3 cells (n=9). (C) Normalized BLI bone metastasis signals. (D) Quantification of CTCs in 100 μl of mouse blood. (E) BLI, X-ray, microCT, histological (H&E and TRAP) and MAOA IHC images of bone lesions (B) invaded by tumors (T) from a representative mouse in each group. Arrows indicate osteolytic bone lesions in X-ray and microCT images, tumor burden in H&E images, and areas of overt bone destruction in TRAP images. In microCT images, regions of interest for trabecular bone scan and analysis are marked by dashed lines; scale bars: 1 mm. H&E, scale bars: 200 μm (low) and 20 μm (high). TRAP, scale bars: 20 μm. MAOA IHC, scale bars: 20 μm. (F) Quantification of tumor areas relative to hind limb in histological sections (n=3). (G) Quantification of radiographic osteolytic lesion areas of hind limbs (n=3). (H) Quantification of bone volume relative to total volume from microCT scans (n=3). (I) Quantification of trabecular thickness from microCT scans (n=3). (J) Quantification of $TRAP^+$ osteoclasts from decalcified histological hind limb sections (n=3). (K) Quantitative IHC analysis of Ki-67 in bone metastases (n=3). Scale bars: 20 μm. Data represent the mean ± SEM. *p<0.05, **p<0.01. See also Figure S2 and Table S2.

Figure 3. Genetic Silencing of MAOA Expression Reduces PCa Metastasis.
(A) Western blotting analysis of MAOA protein levels in control (shCon) and MAOA-KD (shMAOA) C4-2 cells. (B) Kaplan-Meier bone metastasis-free curve of mice inoculated with indicated C4-2 cells (n=10). (C) Normalized BLI signals of bone metastases in (B). (D) Kaplan-Meier survival curve of mice in (B). (E) BLI and X-ray images from a representative mouse in each group in (B). Arrows point to osteolytic lesions. (F) Western blotting analysis of MAOA protein levels in control or MAOA-KD $ARCaP_M$ cells. (G) Kaplan-Meier bone metastasis-free curve of mice inoculated with indicated $ARCaP_M$ cells (n=10). (H) Normalized BLI signals of bone metastases in (G). (I) Kaplan-Meier survival curve of mice in (G). (J) BLI and X-ray images from a representative mouse in each group in (G). Arrows point to osteolytic lesions. (K) Western blotting analysis of MAOA protein levels in control and MAOA-KD PC-3M cells. (L) Kaplan-Meier bone metastasis-free curve of mice inoculated with indicated PC-3M cells (n=9). (M) Normalized BLI signals of bone metastases in (L). (N) Kaplan-Meier survival curve of mice in (L). (O) BLI images from a representative mouse in each group in (L). (P) MicroCT, histological (H&E and TRAP) and MAOA IHC images of bone lesions (B) invaded by tumors (T) from a representative mouse in each group in (B). Arrows indicate osteolytic bone lesions in microCT images, tumor burden in H&E images, and areas of overt bone destruction in TRAP images. Regions of interest for trabecular bone scan and analysis are marked by dashed lines in microCT images, scale bars: 1 mm. H&E, scale bars: 200 μm (low) and 20 μm (high). TRAP, scale bars: 20 μm. MAOA IHC, scale bars: 20 μm. (Q) Quantification of radiographic osteolytic lesion areas of hind limbs from mice in (E) (n=3). (R) Quantification of bone volume relative to

total volume from microCT scans in (P) (n=3). (S) Quantification of trabecular thickness from microCT scans in (P) (n=3). (T) Quantification of $TRAP^+$ osteoclasts from decalcified histological sections of hind limbs in (P) (n=3). (U) Quantitative IHC analysis of Ki-67 in bone metastases from each group in (B) (n=3). Scale bars: 20 μm. Data represent the mean ± SEM. *p<0.05, **p<0.01. See also Figure S3 and Table S2.

Figure 4. MAOA Activates the Shh Pathway in PCa.
(A) *Shh* mRNA levels in 3 pairs of PCa cell lines by RT-qPCR. (B) Shh protein secretion in cell culture media from (A) by ELISA. (C) IHC analysis of Shh protein levels in bone metastases from indicated PC-3 and C4-2 xenografts. Scale bars: 20 μm. (D) Western blotting analysis of Shh protein levels in indicated PC-3 cells. (E) Quantitative analysis of cell invasion and migration in (D). Representative images are shown (left). Scale bars: 200 μm. Quantification of invasive and migratory cells of five distinct images from each replicate (n=3) per group (right). (F) Western blotting analysis of Twist1 protein levels in indicated PC-3 cells. (G, H) *Shh* mRNA levels (G) and protein secretion (H) in cells or culture media from (F) by RT-qPCR and ELISA respectively. (I) Sequences of the canonical Twist1-binding E-box site (top), a putative Twist1-binding E-box site in *Shh* promoter (middle), and introduced point mutations (bottom, italic and red) used to inactivate the E-box site. (J) Alignment of the conserved Twist1-binding E-box element (bold) in *Shh* promoter across different species; numbers indicate distance from transcription initiation site. (K, L) Determination of WT and mutant (Mut) *Shh* promoter activity in indicated PC-3 cells. (M) ChIP analysis of indicated PC-3 cells immunoprecipitated by anti-Twist1 antibody or normal IgG followed by qPCR using primers targeting the Twist1-binding E-box site in *Shh* promoter. Data represent the percent of input. (N) Co-expression correlation analysis of 3 pairs of proteins in a clinical cohort of PCa bone metastatic samples (n=37) by IHC. Images show individual protein staining in representative tumor areas of a high- or low-expression patient sample. Dashed circles indicate tumor (T) and bone (B) areas. Scale bars: 20 μm. Average cell-based staining intensity counts for each individual protein expressed in tumor cells were analyzed by inForm software to assess co-expression correlations. Data represent the mean ± SEM. *p<0.05, **p<0.01. ns, not significant. See also Figure S4 and Table S3.

Figure 5. MAOA Confers Growth Advantages on PCa Cells in the Bone Microenvironment by Shh-Dependent Crosstalk with Osteoblasts.
(A) *Gli* reporter activity in MC3T3-E1 osteoblasts co-cultured with indicated C4-2 tumor cells and treated with DMSO or 20 μM cyclopamine (Cyclo). (B) Shh target gene mRNA levels in MC3T3-E1 co-cultured with indicated C4-2 cells by RT-qPCR. (C) Heat map depicting select TGFβ superfamily ligand gene levels in MC3T3-E1 co-cultured with indicated C4-2 cells by RT-qPCR. (D) Representative images of RFP-tagged C4-2 cell colonies in co-cultures with MC3T3-E1 from each group. White boxes indicate areas shown at higher magnification in the bottom row. Scale bars: 200 μm. (E) Quantification of tumor cell colony diameter in co-cultures in (D). (F) Quantification of luciferase-tagged C4-2 cells in co-cultures with or without MC3T3-E1 by luciferase assay. (G) Quantification of luciferase-tagged C4-2 cells in co-cultures with MC3T3-E1 treated with control, *Gli1* or *Gli2* siRNAs by luciferase assay. (H) *IL6* mRNA levels in MC3T3-E1 cultured alone or separated from indicated co-cultures with C4-2 cells by RT-qPCR. (I) Quantification of IL6 protein secretion in culture media of indicated co-cultures composed of MC3T3-E1 and C4-2 cells by ELISA. (J) Quantification of IL6 protein secretion in culture media of indicated co-cultures combining MC3T3-E1, treated with control, *Gli1* or *Gli2* siRNAs, with C4-2 cells by ELISA. (K) Determination of WT *IL6* promoter activity in MC3T3-E1 co-cultured with indicated PC-3 cells. (L) Sequences of the canonical Gli-binding site (top), a putative Gli-binding site in *IL6* promoter (middle), and introduced point mutations (bottom, italic and red) used to inactivate the potential Gli-binding site. (M) Determination of WT and Mut *IL6* promoter

activity in MC3T3-E1 treated with PBS (vehicle, Veh) or 250 ng/ml recombinant mShh protein. (N) ChIP analysis of MC3T3-E1 treated with conditioned media from indicated PC-3 cells and immunoprecipitated by anti-Gli1 antibody, anti-Gli2 antibody or normal IgG followed by qPCR using primers targeting the Gli-binding site in *IL6* promoter. Data represent the percent of input. (O) Quantification of luciferase-tagged C4-2 cells co-cultured with MC3T3-E1 and treated with 1 μg/ml IL6 antibody or normal IgG by luciferase assay. (P) Quantification of luciferase-tagged C4-2 cells treated with PBS (Veh) or 10 ng/ml recombinant hIL6 protein by luciferase assay. Data represent the mean ± SEM. *p<0.05, **p<0.01. ns, not significant. See also Figure S5 and Figure S6.

Figure 6. MAOA-Expressing Tumor Cells Stimulate Osteoclastogenesis by Shh-Dependently Promoting Osteoblast-Derived RANKL and IL6 Expression.
(A) TRAP staining of pre-osteoclast RAW 264.7 cells treated with conditioned media from co-cultures composed of osteoblasts and indicated tumor cells, treated with DMSO or 20 μM cyclopamine (Cyclo). Arrows indicate mature osteoclasts after differentiation. (B) Quantification of $TRAP^+$ osteoclasts in (A). (C) Quantification of diameter of $TRAP^+$ osteoclasts in (A). (D) *Trap* mRNA levels in RAW 264.7 separated from co-cultures in (A) by RT-qPCR. (E) Heat map of mRNA levels of select osteoclast differentiation markers in RAW 264.7 separated from co-cultures in (A) by RT-qPCR. (F) Quantification of RANKL protein secretion in cell co-culture media of MC3T3-E1 and indicated tumor cells by ELISA. (G) Quantification of $TRAP^+$ osteoclasts in RAW 264.7 treated with conditioned media from co-cultures composed of MC3T3-E1 and indicated PC-3 cells and supplemented with anti-RANKL (5 μg/ml) and/or anti-IL6 (1 μg/ml) antibodies. Data represent the mean ± SEM. *p<0.05, **p<0.01. ns, not significant. See also Figure S7.

Figure 7. Pharmacological Inhibition of MAOA Reduces PCa Metastasis and Prolongs Survival in Mice.
(A) Kaplan-Meier bone metastasis-free curve of mice treated with vehicle (Veh, saline) or clorgyline (Clg) (n=9). (B) Normalized BLI signals of bone metastases. (C) Kaplan-Meier survival curve of mice. (D) BLI and X-ray images of a representative mouse from each group. Arrows point to osteolytic lesions. (E) MicroCT and histological (H&E and TRAP) images of bone lesions (B) invaded by tumors (T) from one representative mouse in each group. Arrows indicate osteolytic bone lesions in microCT images, tumor burden in H&E images, and areas of overt bone destruction in TRAP images. In microCT images, regions of interest for trabecular bone scan and analysis are marked by dashed lines; scale bars: 1 mm. H&E, scale bars: 200 μm (low) and 20 μm (high). TRAP, scale bars: 20 μm. (F) Quantification of radiographic osteolytic areas of hind limbs (n=6). (G) Quantification of bone volume relative to total volume from microCT scans (n=3). (H) Quantification of trabecular thickness from microCT scans (n=3). (I) Quantification of $TRAP^+$ osteoclasts from decalcified histological sections of hind limbs (n=3). (J) Quantitative IHC analysis of Ki-67 in bone metastases (n=3). Scale bars: 20 μm. (K) mRNA levels of Shh target genes and other select bone metastasis-promoting genes in the bone metastasis stromal compartment of mice by RT-qPCR. (L) IHC images of MAOA, Shh, Twist1 in tumor areas and IL6, Gli1, Gli2 in tumor-associated bone stromal areas from serial sections of high- or low-expression patient samples. Dashed circles indicate tumor (T), bone (B) and stromal (Str) areas. (M) Co-expression correlation analysis of protein pairs in a PCa bone metastasis patient cohort (n=37). (N) Schematic depicting the interactions of MAOA-expressing tumor cells with the bone microenvironment mediated by MAOA and associated Shh-IL6-RANKL paracrine signaling network. Data represent the mean ± SEM. *p<0.05, **p<0.01. See also Figure S3, Figure S7 and Table S3.

Figure 1 (Wu *et al*)

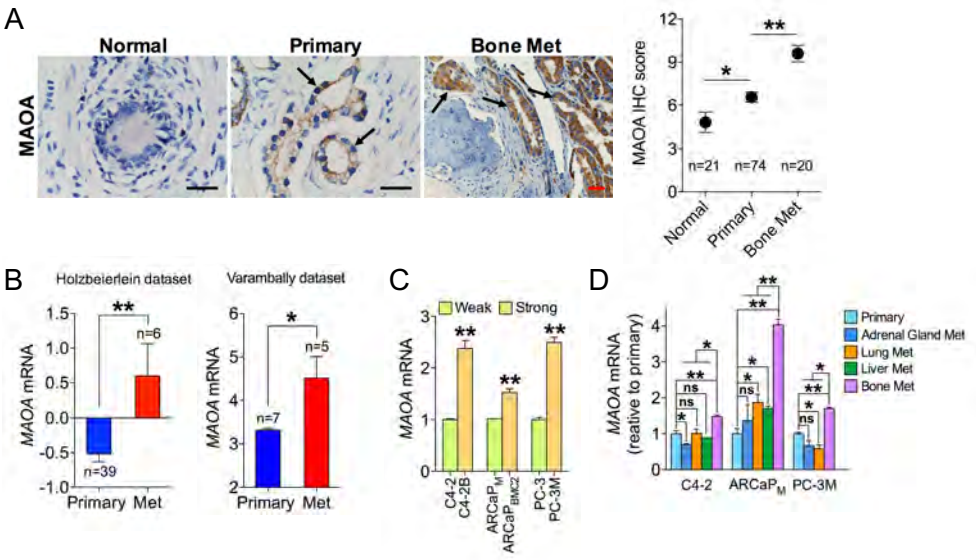

Figure 2 (Wu *et al*)

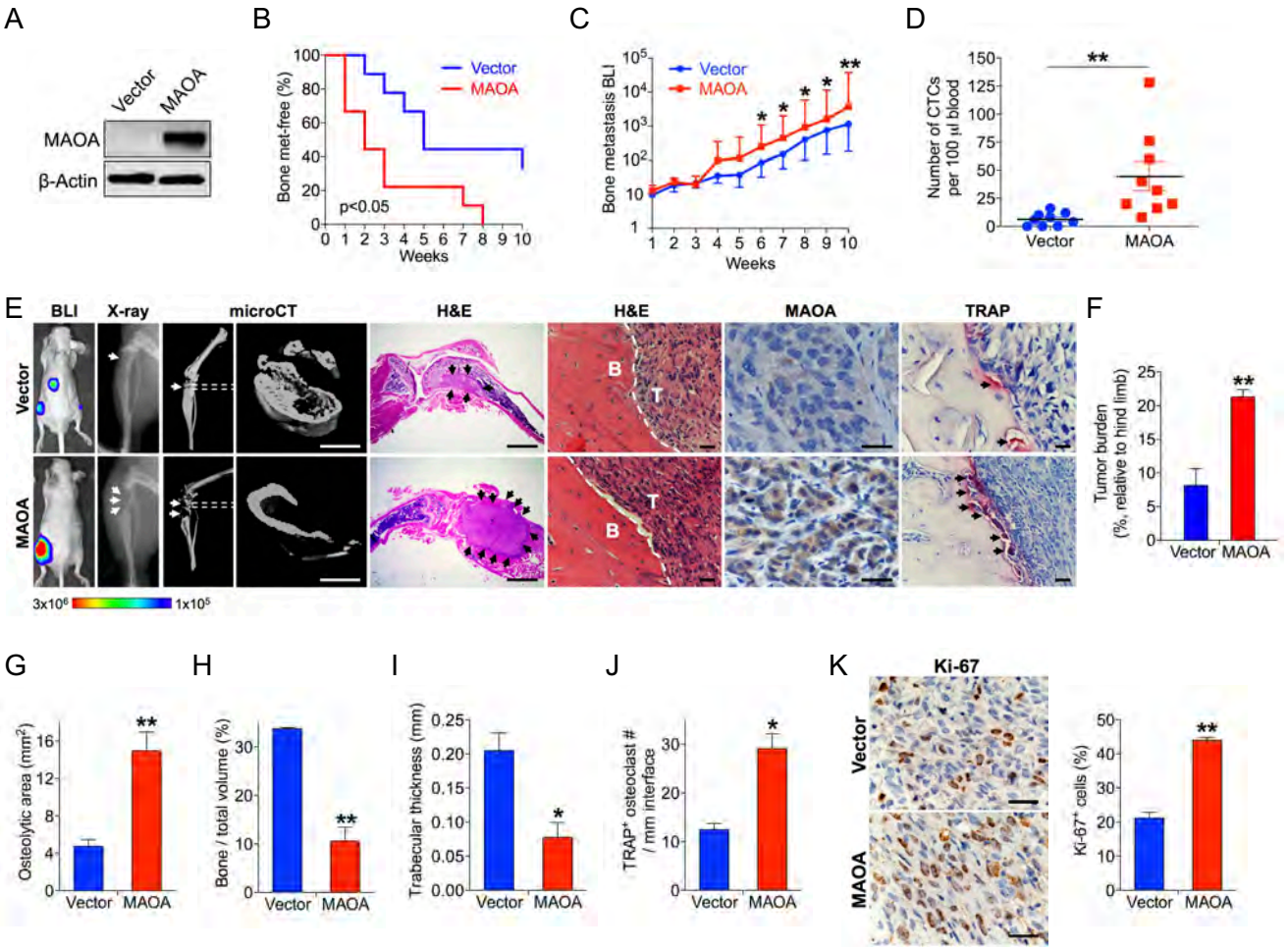

Figure 3 (Wu *et al*)

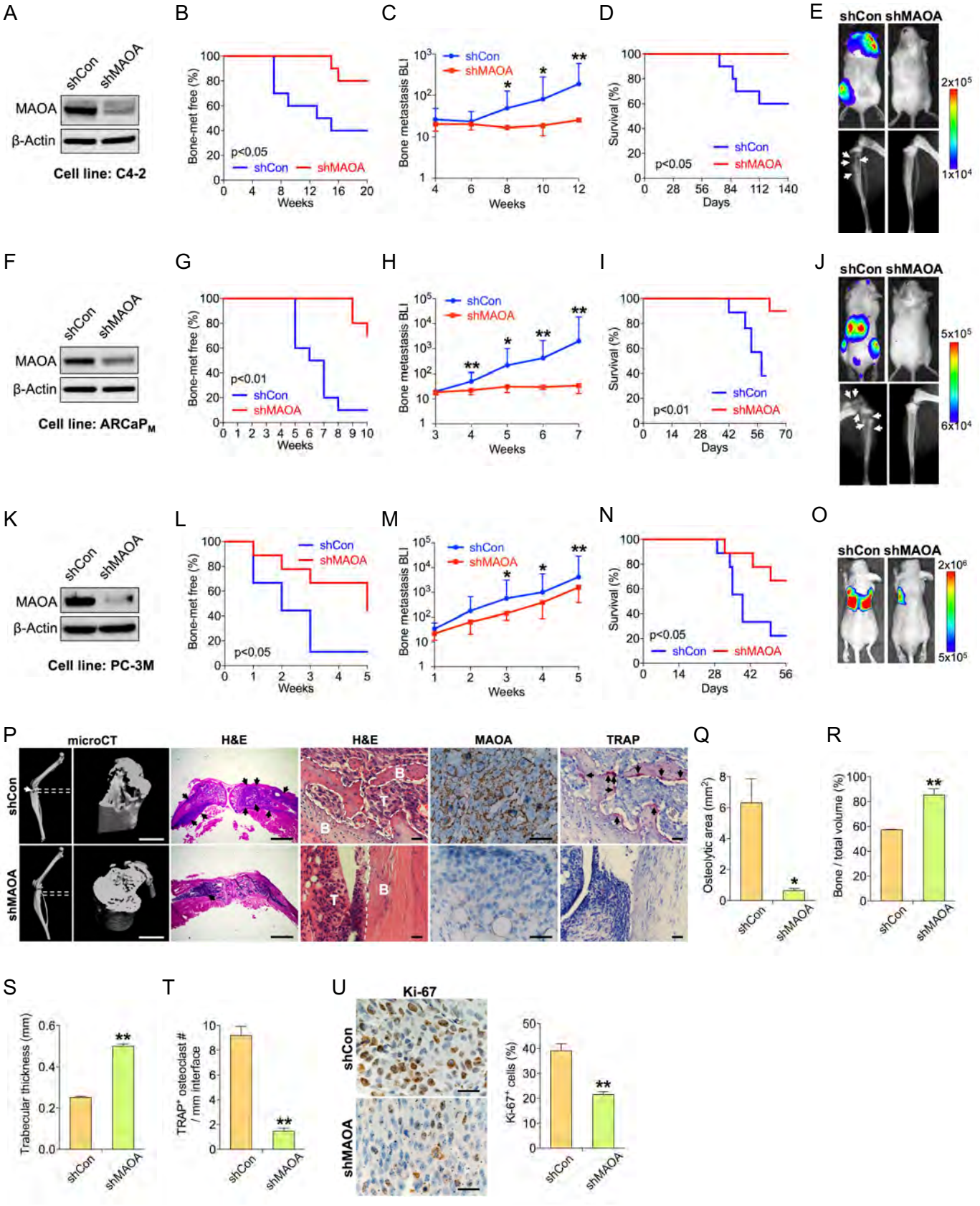

Figure 4 (Wu *et al*)

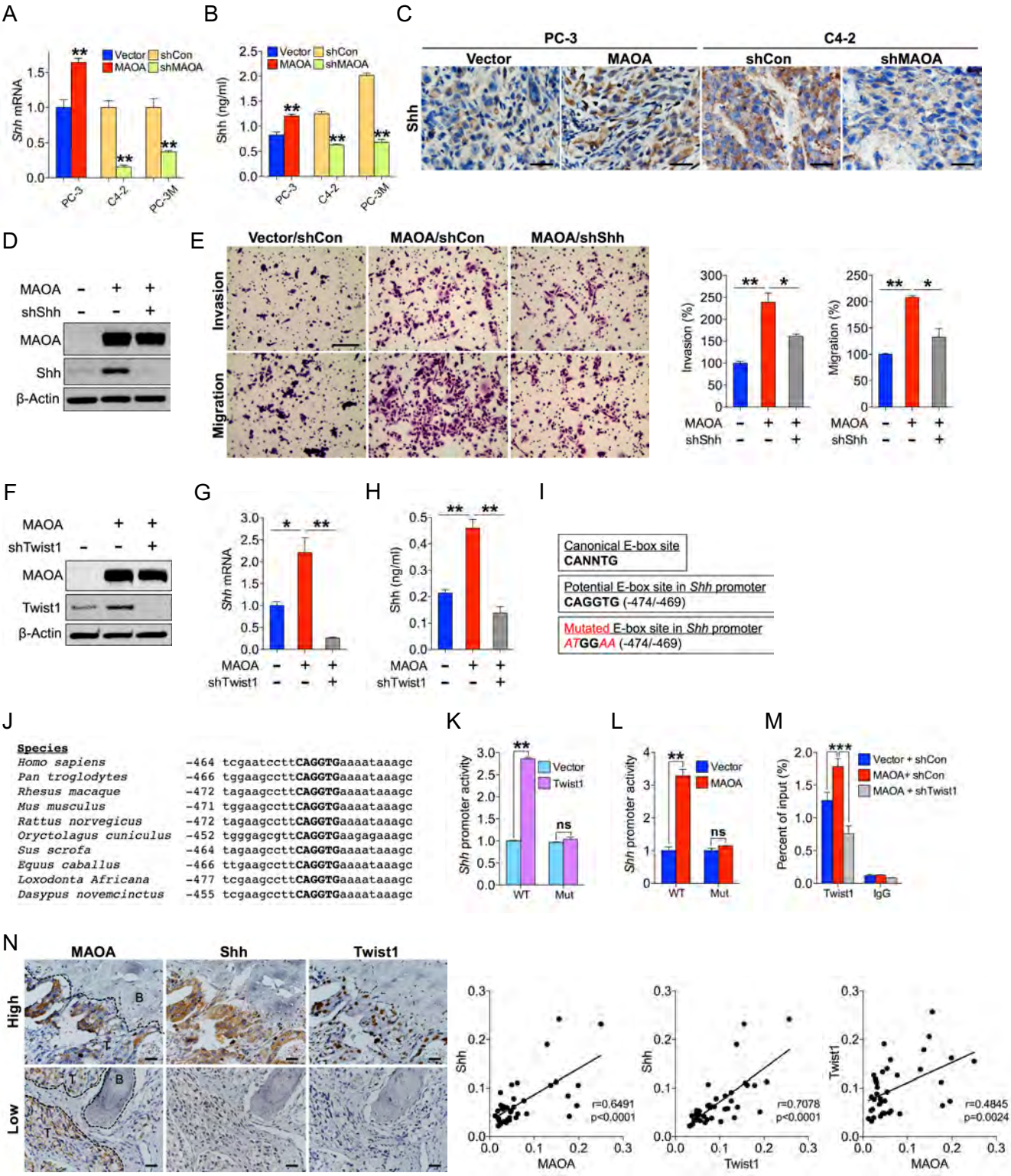

Figure 5 (Wu *et al*)

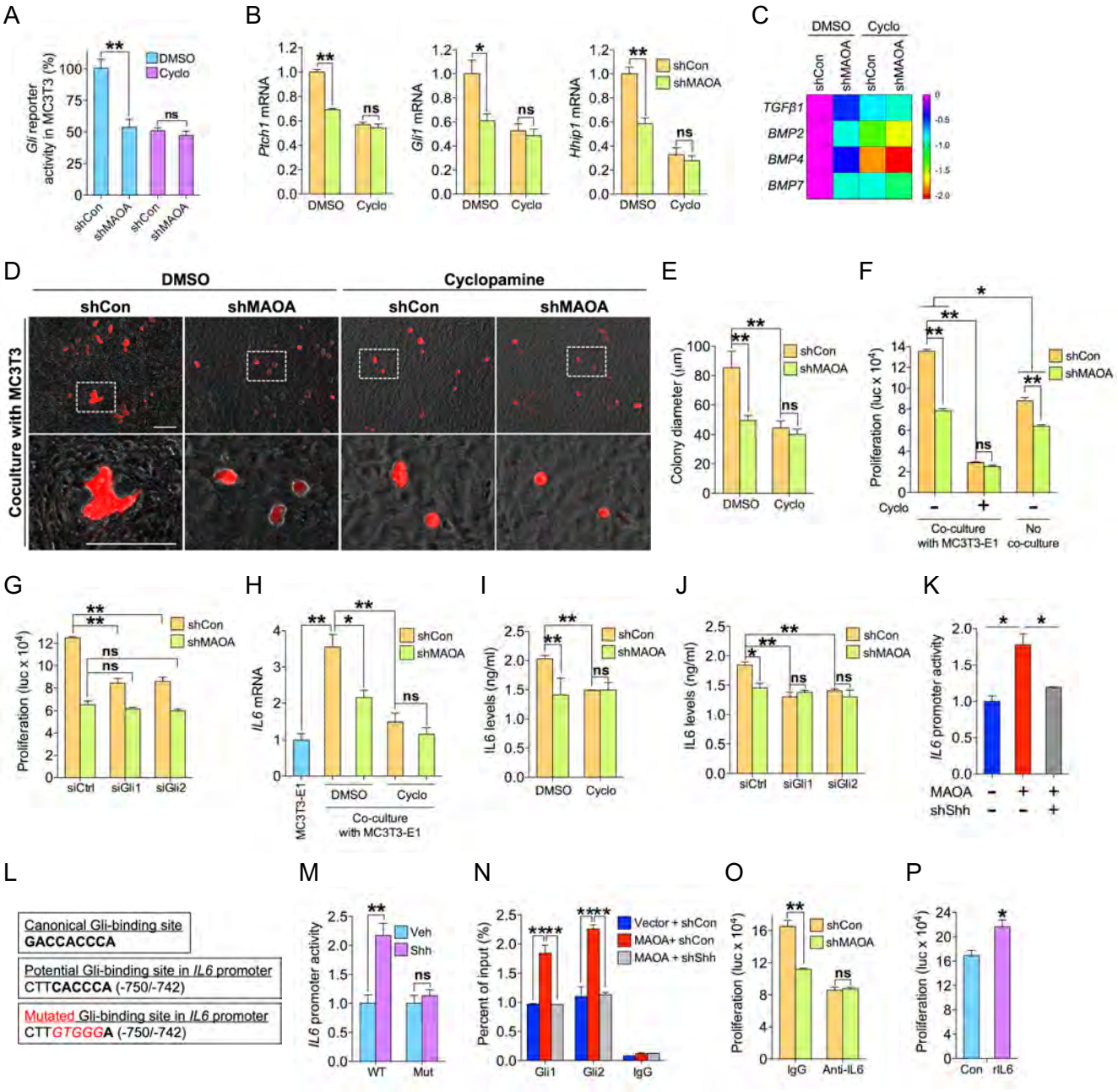

Figure 6 (Wu *et al*)

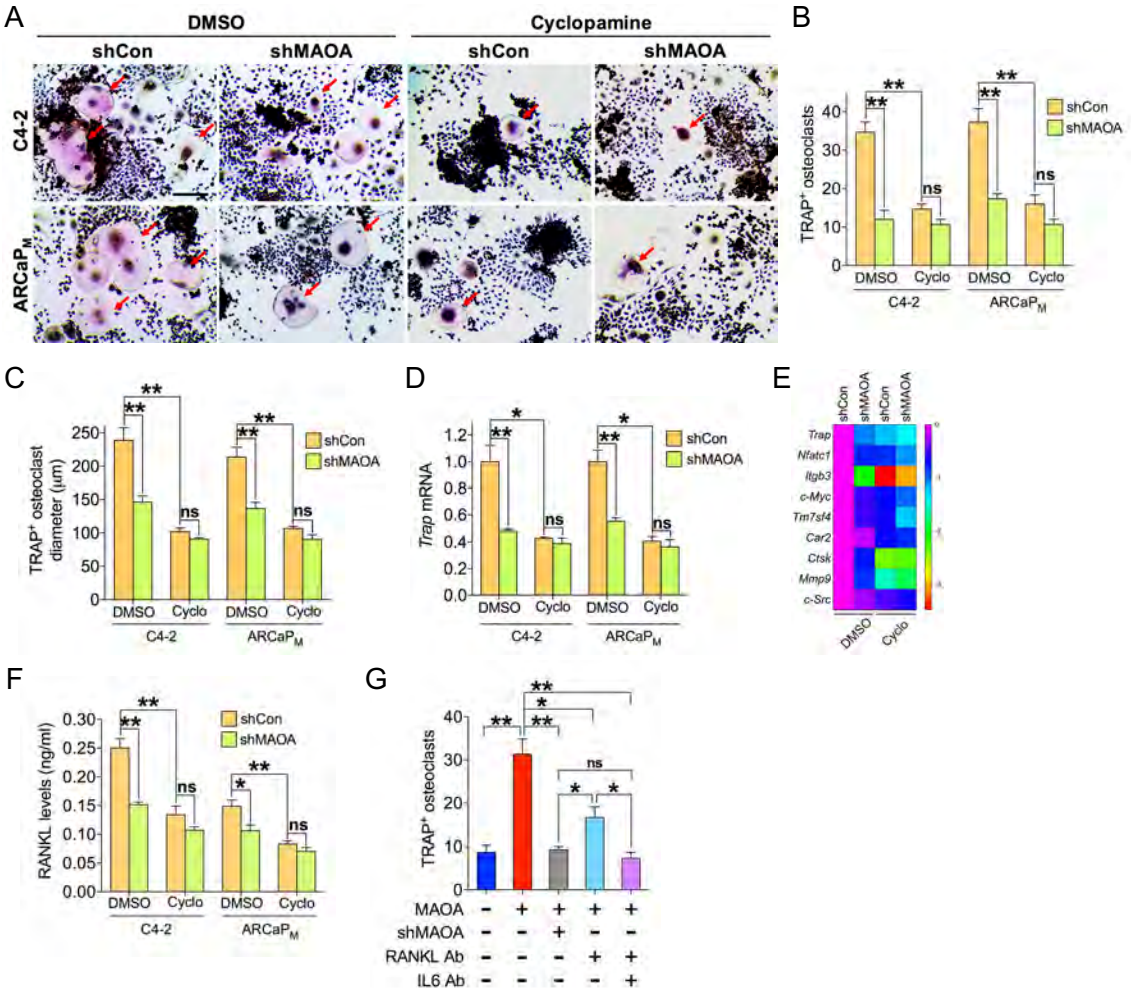

Figure 7 (Wu *et al*)

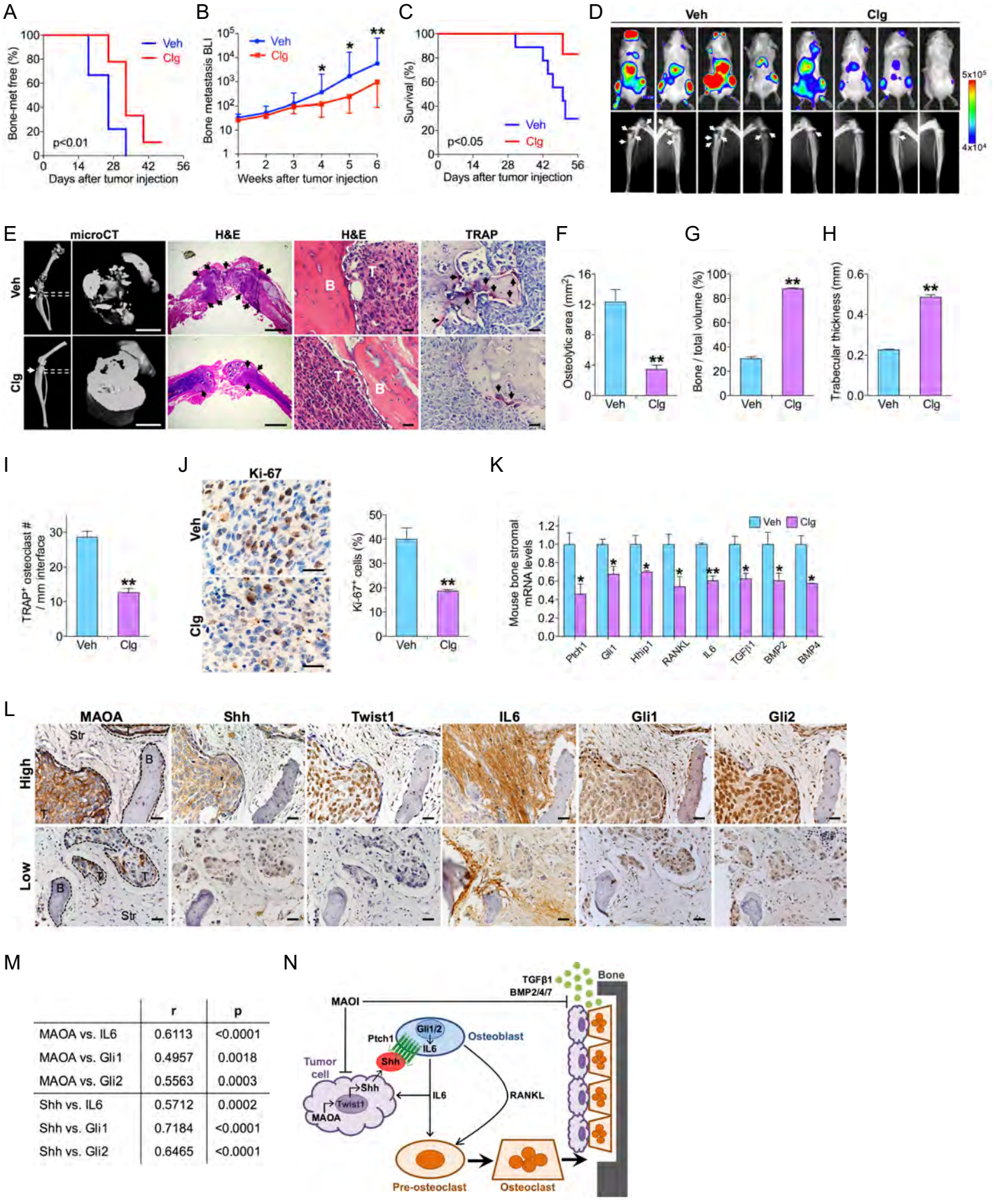

	r	p
MAOA vs. IL6	0.6113	<0.0001
MAOA vs. Gli1	0.4957	0.0018
MAOA vs. Gli2	0.5563	0.0003
Shh vs. IL6	0.5712	0.0002
Shh vs. Gli1	0.7184	<0.0001
Shh vs. Gli2	0.6465	<0.0001